KERNFORSCHUNGSANLAGE JÜLICH GmbH

Programmgruppe
Systemforschung und Technologische Entwicklung

Angewandte Systemanalyse
Nr. 26

Plastic Solar Air Heaters of a Novel Design - Testing and Performance -

von

Bansal, N. K.
Uhlemann, R.,
Boettcher, A.

Jül - 1783
April 1982
ISSN 0366-0885

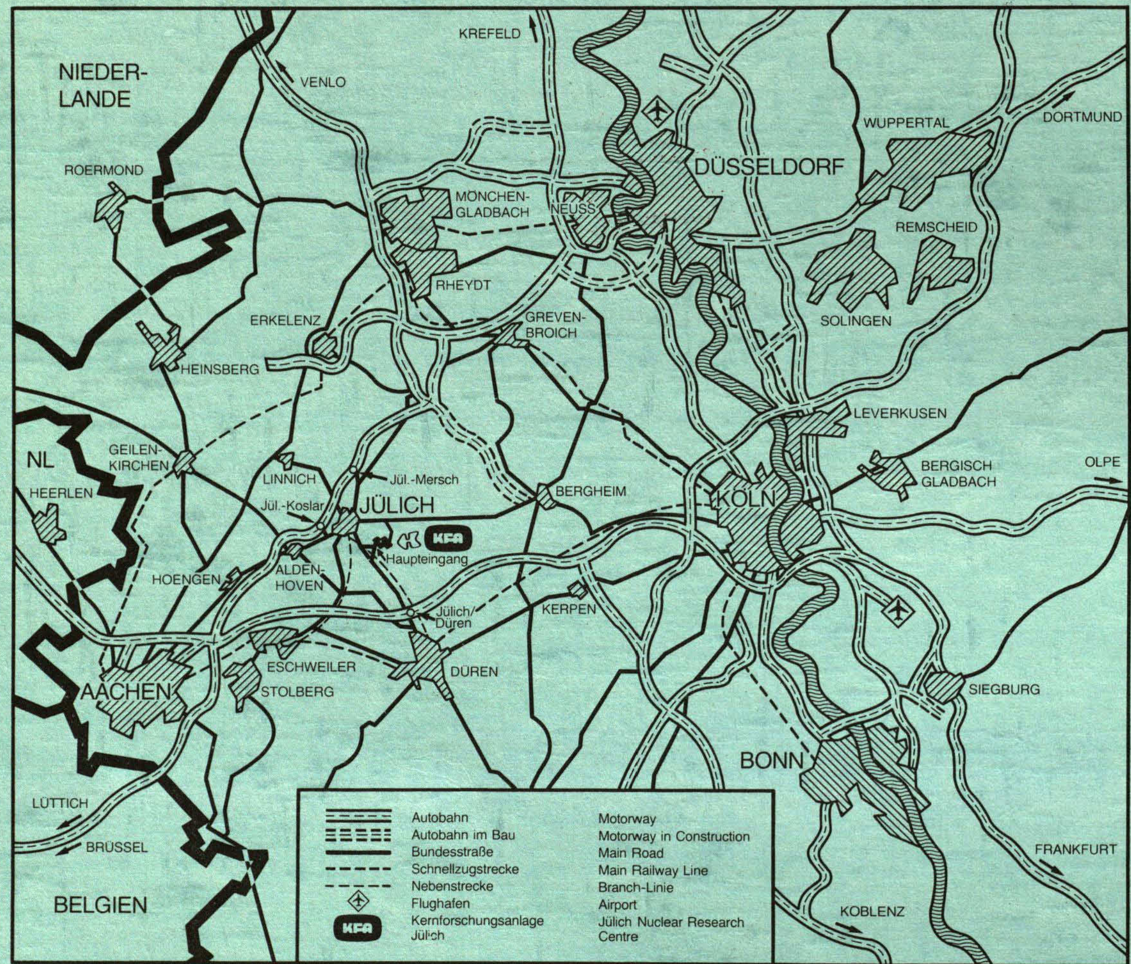

Als Manuskript gedruckt

Berichte der Kernforschungsanlage Jülich - Nr. 1783

Programmgruppe Systemforschung und Technologische Entwicklung Jül - 1783

Zu beziehen durch: ZENTRALBIBLIOTHEK der Kernforschungsanlage Jülich GmbH

Postfach 1913 · D-5170 Jülich (Bundesrepublik Deutschland)

Telefon: 02461/610 · Telex: 833556 kfa d

Angewandte Systemanalyse
Nr. 26

Plastic Solar Air Heaters of a Novel Design
- Testing and Performance -

von

Bansal, N. K.
Uhlemann, R.,
Boettcher, A.

NEUARTIGE SOLAR-LUFTKOLLEKTOREN AUS KUNSTSTOFF - MESSUNG DES THERMISCHEN VERHALTENS

N.K. Bansal+), R. Uhlemann, A. Boettcher++)

KURZFASSUNG

Der Aufbau und erste Versuchsergebnisse von neuartigen, ganz aus Kunststoff gefertigten, flexiblen Solar-Luftkollektoren mit porösem Absorber sowie das hierzu entwickelte Meßverfahren werden beschrieben. Typische Anwendungsmöglichkeiten für diese Kunststoffkollektoren liegen im Agrarbereich, wie die Trocknung von Ernteprodukten, jedoch auch Brauchwassererwärmung und Raumheizung gehören dazu.

Für unsere Versuche wurden drei verschiedene Kollektoren dieses Typs angefertigt, von denen zwei eine Länge von etwa 10 m und eine Breite von 1 m haben, sich jedoch im Kunststoffgewebe des Absorbers, das von verschiedenen Firmen stammt, unterscheiden. Der dritte Kollektor ist 20 m lang und wurde vermessen, um den Effekt unterschiedlicher Kollektorlängen zu untersuchen.

Der thermische Wirkungsgrad der Kollektoren wurde in Abhängigkeit von den typischen Parametern, Luftmenge, solare Einstrahlung, dem Absorbegewebetyps sowie der Dicke der rückseitigen Isolierung gemessen. Um ein qualitatives Verständnis der Luftströmung und Wärmeübertragung im Kollektor bei den verschiedenen Absorbegeweben zu gewinnen, wurden die Luftdruck- und Temperaturverteilung über die Länge oberhalb und unterhalb des Absorbertuches gemessen.

Für identische Umgebungsbedingungen und identische Luftmenge zeigt sich der Wirkungsgrad stark abhängig von der Art des Absorbegewebes und der rückseitigen Isolierung des Kollektors. Die besten Ergebnisse lassen sich mit einem der 10 m Kollektoren bei einer 6 cm starken rückseitigen Isolierung aus wasserabweisendem Polyäthylenenschaum erzielen. Bei einer solaren Einstrahlung von 687 W/m^2 in der Kollektorebene ergibt sich bei einem Volumenstrom von 800 m^3/h Luft durch den Kollektor eine Temperaturerhöhung von 16,6^0 C und damit ein Wirkungsgrad von etwa 71 % oder eine nutzbare thermische Leistung von 4,5 KW.

Die theoretische Betrachtung des Kollektors zeigt, daß die in der Temperatur lineare Hottel-Whillier-Bliss Gleichung zu falschen Werten für die Kollektorgrößen Wärmeverlustkoeffizient U_L, effektiver Transmissions-Absorptionsfaktor $(\alpha\cdot\tau)_e$ und Kollektorwirkungsgradfaktor F' führt, wenn es sich um stark poröse Absorberstrukturen handelt. Für das dichtere Absorbergewebe führt die lineare Näherung, wie gewöhnlich, zu korrekten Werten für die charakteristische Größen des Kollektors.

+) Gastwiss. vom Indian Institute of Technology, Delhi, India
++) Internationales Büro der KFA Jülich

PLASTIC SOLAR AIR HEATERS OF A NOVEL DESIGN - TESTING AND PERFORMANCE

N.K. Bansal+), R. Uhlemann, A. Boettcher++)

ABSTRACT

A novel design of solar air heaters of porous type made completely from plastic materials has been forwarded for typical applications like crop drying, domestic water and space heating etc. An experimental test facility brought up to study the thermal performance of these collectors has been described.

Three collectors, each having a width of about one meter, were fabricated for testing purposes. Two of these collectors have identical length of approximately ten meters but the absorber, which is a textile, was obtained from two differrent firms. The third collector is twenty meters long and was essentially made to study the effect of length. A detailed study was undertaken to determine the variation in the thermal performance of these collectors with typical parameters like quantity of the flowing air, solar insolation, absorber type and back insulation, etc. For identical ambient conditions and for a fixed air flow, the performance of the collectors is found to be dependent very sensitively on the kind of textile absorber and the insulation at the back.

For the better 10 m long collector a high thermal performance is achieved if one keeps a 6 cm thick polyethylene insulation at the back of the collector. For an incident solar radiation of 687 w/m^2 at the collector surface, one is able to achieve a temperature rise of 16.6^o C in the air flowing through the solar collector at a rate of 800 m^3/h, thus yielding an efficiency of nearly 71 % and useful thermal power of about 4.5 kW.

Further it is seen that the linear approximation for the Hottel-Bliss equation leads to erroneous estimations for the collector parameters, like the total heat loss coefficient U_L, plate efficiency factor F' and the effective $(\alpha\tau)_e$ product, when the absorber is porous. For a dense absorber, however, such an approximation yields, as usual, correct numerical values for the characteristic parameters of the collectors.

+) on leave from Indian Institute of Technology, Delhi, India
++) Internationales Büro der KFA Jülich

CONTENTS

1 INTRODUCTION

The potential applications of solar air-heaters are domestic hot water and space heating, drying of agricultural products and lumber under controlled conditions, heating of greenhouses etc. In contrast to vast studies on water heating collectors, the studies on the design and performance of air heaters have been rather limited. The difficulties often encountered with air heating collectors are the limitations of heat transfer from the absorber plate to the working fluid and the need to handle large volumes of air than liquids due to the low density of air as the working substance. Several designs of solar air heaters have been proposed for improving their thermal performance and some of them have yielded good results /1, 2/.

The designs of solar air heaters forwarded so far can basically be classified into two categcries. The first type has a nonporous absorber in which the air stream does not flow through the absorber plate. Air may flow above and/or behind the absorber plate. The second type has a porous absorber that includes slit and expanded metal, transpired honey-comb and overlapped glass plate absorber. The utility of the later type over the former one consists in providing a lower pressure drop across the collector and also reducing thermal losses to the environment because the solar radiation in this case penetrates to greater depths and is absorbed gradually depending upon the matrix density /1/. The studies on nonporous air heaters have been made by Whillier /3/, Close /4/, Khanna and Singh /5/, and Gupta and Garg /6/, Bansal and Kaushik /7/ and Parker /8, 9/ etc. Porous matrix type air heaters have been extensively analysed and tested by Chiou et al /10/, Beckmann /11/, Hamit and Beckmann /12/, Selcuk /13, 14/, Akyurt et al /15/, Lansing et al /16/, Singh et al. /17/ and Sodha et al /18/.
In most of these studies the material used for the absorber plate was that of metal and for glazing one used either glass or plastic sheets. The cost of the collector therefore did not come out to be much cheaper than those of water heating collectors.

One of the ways to make the solar heating economically attractive is to use the plastic materials in the manufacture of various components. A review listing various plastic materials suitable for various components of a solar energy collector has been given by Blaga /19/ and Boeckmann /20/. The procedure of making thin films of the plastic on the absorber and over the cover has been described by Andrews and Wilhelm /21/. The solar air heating collectors made completely from the plastic material include those of Wilhelm /21/, Weichman and Hughes /22/, Sarazin and Olson /23/, Chio /24/, Erb /25/, Hoynowski /26/, Kay /27/, Boettcher and Delyannis /28/ and Schulz /29/. The plastic collectors constructed from the plastic materials so far have been mainly of nonporous type which can abviously reach a limited efficiency and have the disadvantage of providing high pressure drop across the collector.

In this communication we present a detailed study of porous type of air heating solar collectors made from plastic material and which are capable of handling large volume of air. The design of the collector has been described in Section 2. Three different collectors, two of 10 m length and another of 20 m length have been fabricated by Dynamit Nobel.*

---

* *Dynamit Nobel, 521 Troisdorf, West Germany*

The detailed dimensions along with typical physical parameters of the three collectors are described in table 1 of section 2. To test the collectors an outdoor facility was set up at the terrace of the institute (STE) and the measurements of the relevant quantities were done on a MADAS /33, 37/ data processing system. The details of the test facility and experimental set up are described in section 3.

Section 4 deals with the relevant performance equations and in section 5 we present the results of measurements and calculations.

2 DESIGN OF THE COLLECTORS

The present collector belongs to the category of porous absorbers and is fabricated from flexible plastic sheets. As an absorber there is a porous black textile of polyester (100 %) and it is attached to two transparent sheet of polyvinyl chloride (PVC) at the edges and is covered by them from both the sides (Fig. 1). The edges of the collector have ring holes at a distance of 0.50 m from each other for fixing the collector on the stand (described in section 3). The transparent PVC sheet which acts as cover is 0.6 mm thick and has about 83 % transmittance for global solar radiation and the material is stabilized against ultraviolet radiation. The measured transmittance* of the present PVC sheet in the spectral range 9-20 μm is very low (∼ 6 %) (Fig. 2). Thus for absorber temperatures in the range 40 - 100 °C this PVC sheet acts as an excellent cover. The lower PVC sheet is provided to double the life time of the collector; when the top cover becomes opaque to solar radiation due to natural effects then the collector is simply inverted so that the bottom PVC sheet now acts as a cover.

The porous textile in the collector should be so selected as to have maximum absorption of solar radiation but allowing a good flow of air through it. Since the air flows over the entire absorber area the pressure drop across the collector in such constructions is much lower than in the case of nonporous absorbers. Simultaneously, since the radiation is absorbed by different layers over the thickness of the absorber, the upper layer is not at the maximum temperature resulting in reduced thermal losses. Presently we got three collectors fabricated. Two of them are of approximately 10 m^2 area each and the other is of about 20 m^2 area. The width of the black textile in each case is about 1 m, while the top and bottom PVC covers are made slightly bigger. With this construction the absorber lies flat after fixing while the air is contained between the top PVC sheet and textile respectively, before and after getting heated. Our two 10 m^2 area collectors have two different textiles found most suitable from preliminary measurements. A twenty times enlarged surface photograph of the two textiles taken from an electron microscope is given in Figures 3a and 3b respectively. One 10 m^2 area collector (called 10 m collector a later) has the textile of Fig. 3a as the porous absorber. This textile was found to transmit about 8 % of the solar radiation. The absorptance of the absorber is therefore approximately 88 % assuming 4 % reflection losses from its surface. Another 10 m^2 area collector (called 10 m collector b

---

* *Transmittance measurements were performed at the Indian Institute of Technology, Delhi, India*

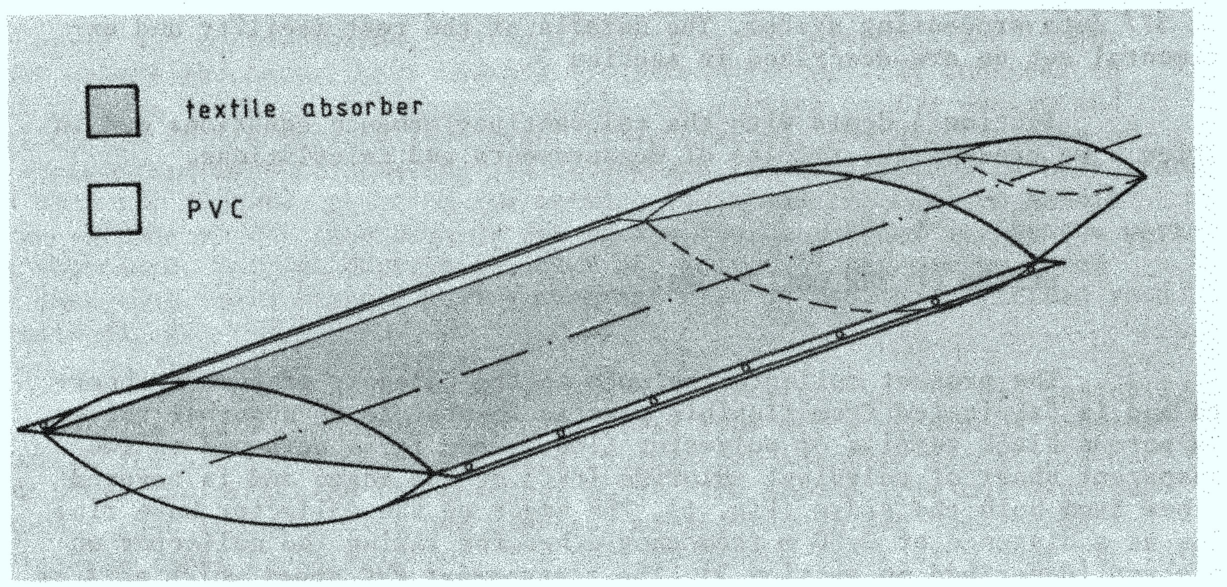

Fig.1: Diametric section of the air collector

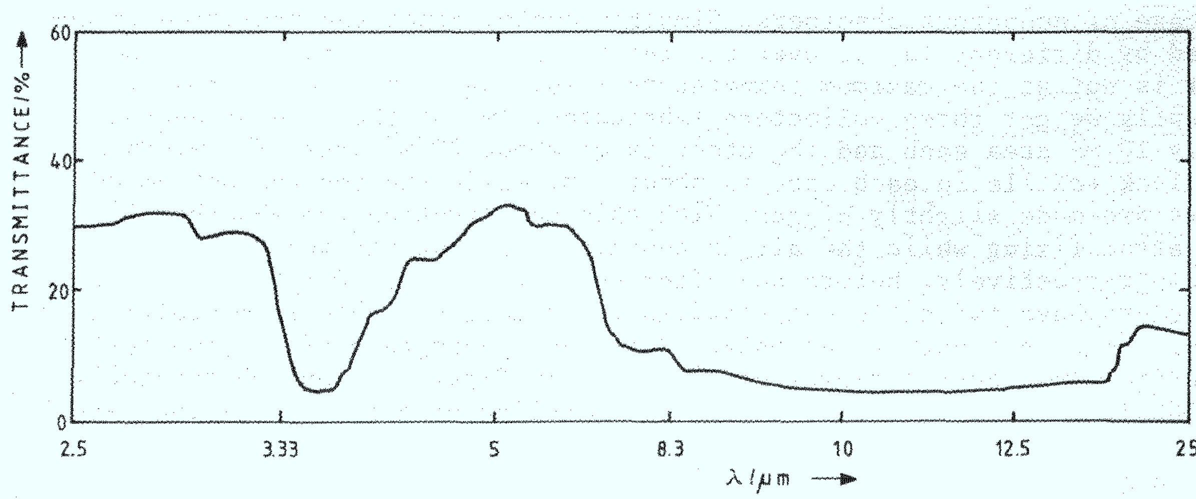

Fig.2: Measured transmittance of PVC-cover in the wavelength region of 2.5 - 25 μm (cover thickness 0.6 mm)

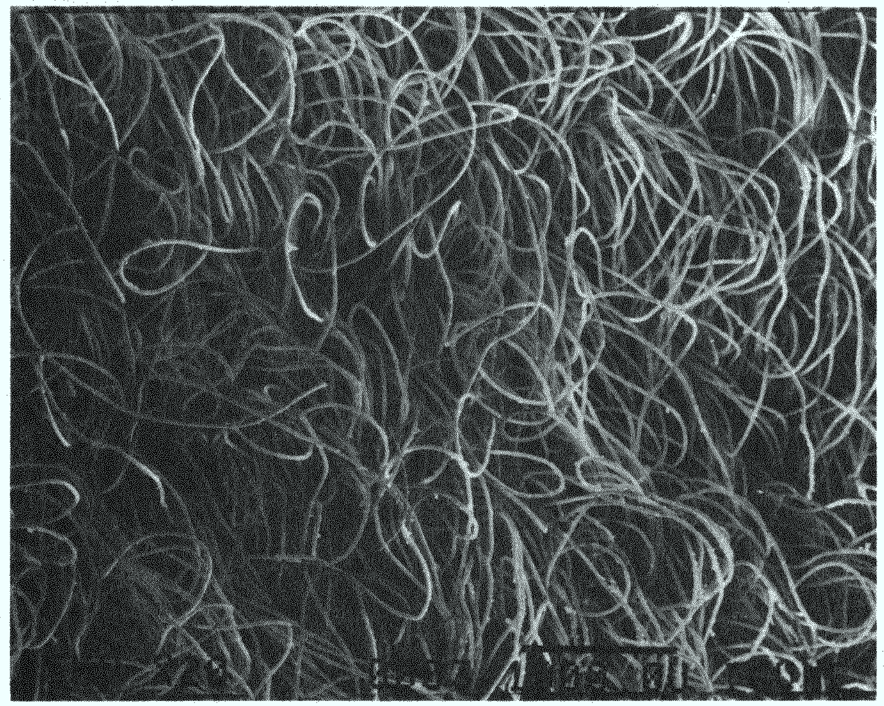

Fig. 3a: Surface structure of the textile absorber of 10 m collector a
(20 times magnified electron microscope photograph)

Fig. 3b: Surface structure of the textile absorber of 10 m collector b and 20 m
collector (20 times magnified electron microscope photograph)

(e.m. photographs of the textile surface were made at IGV/KFA-Jülich) later) and 20 m^2 area collector (called 20 m collector later) have the textile of Fig. 3b as the absorber. This textile (Fig. 3b) is found to absorb 78 % of the solar radiation. The details of each of the collectors about their geometry and relevant physical parameters are given in table 1.

Table 1: Dimensions and physical properties of the plastic collectors

Items	10m collector a	10m collector b	20m collector
length of the collector	8.85m	8.80m	17.60m
width of the collector	1.03m	1.15m	1.13m
absorbing area	9.12m^2	10.12m^2	19.89m^2
cross-section of the collector at the inlet and outlet of the air	0.061m^2	0.061m^2	0.061m^2
material of the cover	PVC	PVC	PVC
thickness of the cover	0.6mm	0.6mm	0.6mm
transmittance τ of the PVC-cover in the solar spectrum range	0.83	0.83	0.83
transmittance in the wave-length range 9-20μm	0.06	0.06	0.06
material of the absorber	100% Polyester	100% Polyester	100% Polyester
tissue	textile No.: 12503*	textile No.: 2262/180**	Textile No.: 2262/180**
thickness of absorber tissue	~2mm	~2mm	~2mm
transmittance of the textile absorber for solar radiation	0.08	0.22	0.22

** Firm. Säckinger Feinwirkerei, 7880 Säckingen/Rhein, FRG

3 EXPERIMENTAL SET UP AND MEASURING INSTRUMENTS

The test facility for testing the solar air collector is schematically shown in Fig. 4. It consists of the following set up.

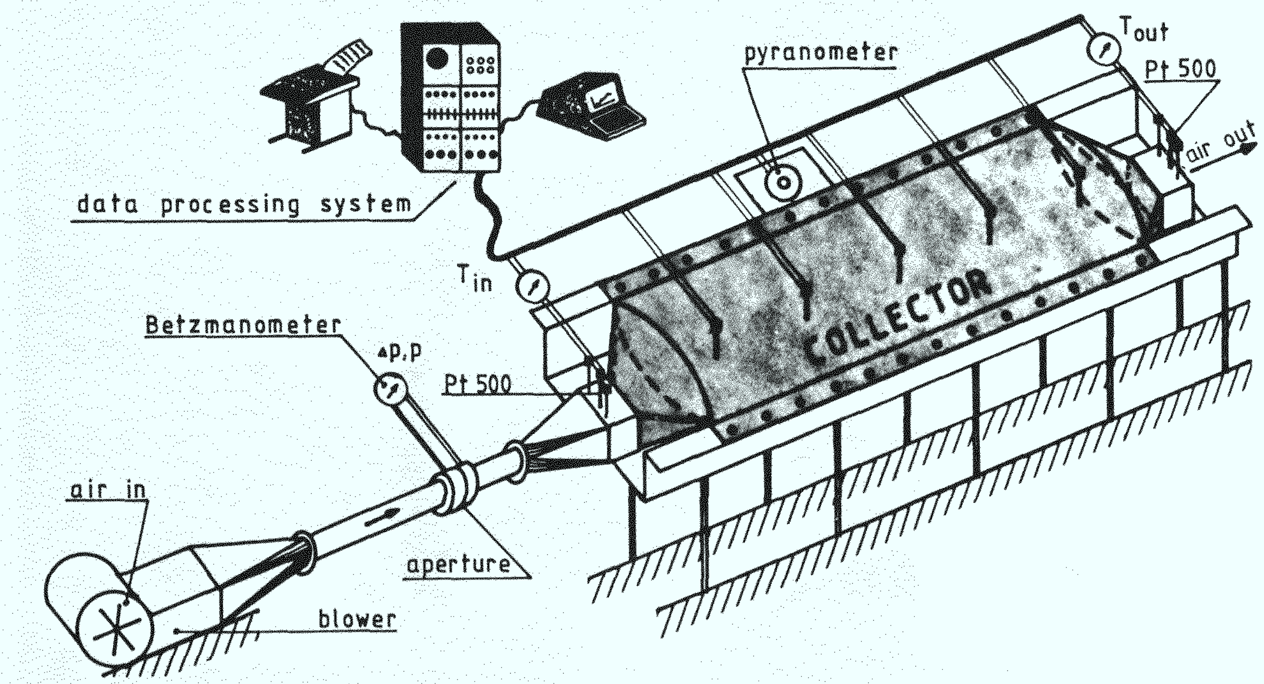

Fig.4: Schematic of Test Facility

3.1 Stand for framing the collector

The collector being flexible has to be put very properly and stretched in such a position so as to receive maximum solar radiation. The frames on which the collector was to be fixed were 5 meters long and 1.50 m wide. The frames were fixed on 5 tables oriented towards south with the possibility of changing the angle which was kept 45^o for the present study.** They were covered with wood and polyethylene insulation of 3 cm thickness initially. The collector was fixed over the insulation. A photograph of the completed test facility is given in Fig. 5.

3.2 Blower

The blower used for letting the air flow inside the collector is a Lau forward curved blower /30/ from the firm Fischbach* of type D570/E280. The details of the blower are as follows:

---

* *Fischbach, D-5908 Neunkirchen, West Germany*
** *Latitude of Jülich is $\phi = 50^o\ 55'\ 33''$ north*

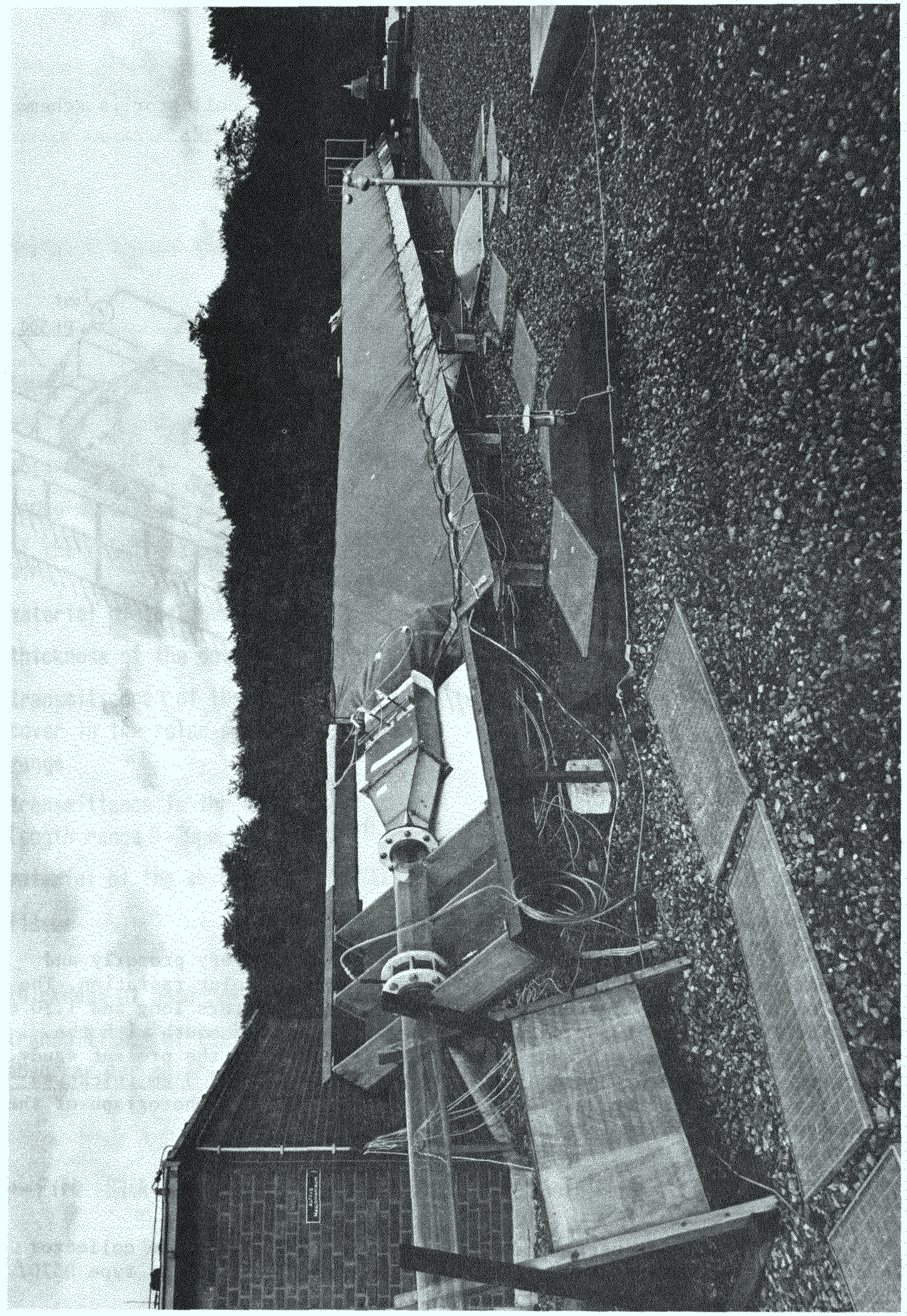

Fig. 5: A view of the test facility for long plastic solar air heaters at KFA-STE

Absolute electrical power	0.25 kW
Electrical potential variation	30 - 220 V
R.P.M.	0 - 1410 t/min
Max. Temp. for free operation	60 °C

Maximum air volume rate at free blowing operation:

$\dot{m}_{max}$ 2850 m^3/h

3.3 Air flow measurement

The measurements of the quantity of air flowing through the collector were performed by an accurate technique* of measuring the pressure drop across a nozzle. The nozzle and the corresponding track shown in Fig. 6 were fabricated by the firm DEBRO** according to the specifications of

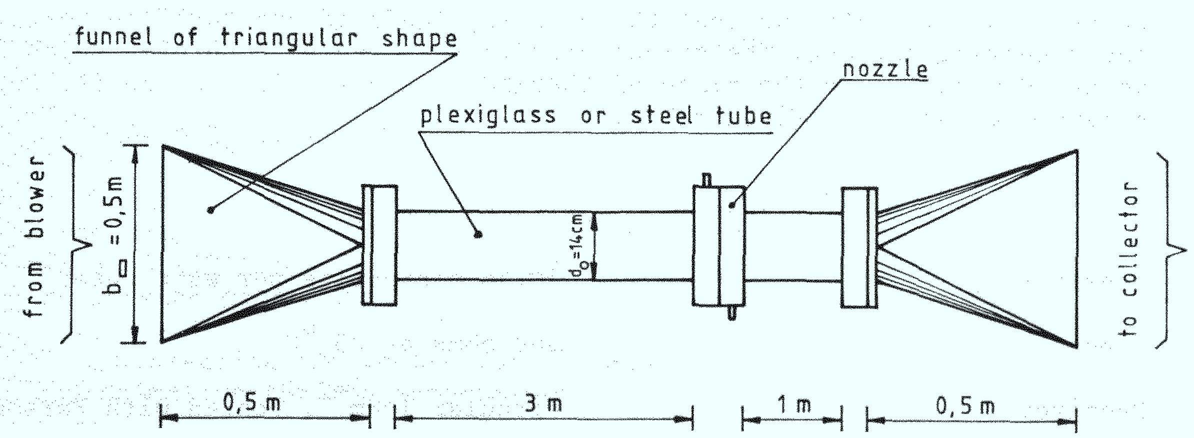

Fig.6: Track specifications for air flow measurements

---

* *It is our experience that measuring the air speed with an anemometer and then multiplying it by the density of air and cross section of the outlet to get the rate of the flowing air in kg/s results in overestimates. Thus often high efficiencies have been reported in literature /16, 29/.*

** *DEBRO-Meßtechnik, 4005 Meerbusch 1, West Germany*

DIN* 19205 /31/. The introduction of a multinozzle plug between the manometer and the nozzle enables to measure the static pressure also.

The amount of air $\dot{m}$ flowing through the collector is calculated by using the following equation

$$\dot{m}_w = \delta \cdot \varepsilon \cdot A_d \cdot \sqrt{2 \cdot \Delta P \cdot \rho}$$

where the flow rate number δ and the expansion factor ε both are functions of the Reynold number and the dimensions of the measuring track. For the aperture supplied to us and for our measuring track $\dot{m}$ is simply calculated by the formula

$$\dot{m} = 111.11 \cdot h^{1/2} \quad (1)$$

where h is the pressure drop across the nozzle measured by the manometer. in mm H_2O.

3.4 Radiation Measurements

The total solar insolation on the collector is measured by an Eppley pyranometer (Model PSP) by mounting it at the same inclination as the collector. Precautions have been taken to avoid subjecting the instrument to mechanical shocks or vibrations during the installation. The pyranometer is orientated so that the emerging leads (connector) lie north of the receiving surface. The pyranometer is supplied with shields which are adjusted parallel to the plane of thermopile and lie just below it. Eppley pyranometer data are given below.

Instrument characteristics

Sensitivity	10.58 microvolts per watt meter^{-2}
Impedance	668 ohms at 23 ^{o}C
Receiver	circular 1 cm^{-2}, coated with Parsons' black optical lacquer
Temperature dependence	1 per cent over ambient temperature range -20 to +40 ^{o}C (temperature compensation of sensitivity can be supplied over other ranges at additional charge)
Linearity	0.5 per cent from 0 to 1400 watts m^{-2}

---

* *Deutsche Industrie Norm*

Response time	1 second (1/e signal)
Cosine	1 per cent from normalization 0 - 70 zenith angle 3 per cent 70 - 80^{o} zenith angle
Orientation	no effect on instrument performance
Mechanical vibration	tested up to 20 g's without damage
Calibration	integrating hemisphere (approx. 1 cal cm^{-2} min^{-1}, ambient temperature +25 ^{o}C): calibration reference Eppley primary standard group of Angstrom pyrheliometers reproducing the International Pyrheliometric Scale
Readout	Potentiometric in preference to microammeter devices

3.5 Temperature Measurements - General

Temperatures are being measured with the help of Pt 100 and Pt 500 resistance temperature sensors which have been fixed in a copper tube with a plug at the other end in a manner shown in Fig. 7a and 7b. As is evident a 4 wire technique has been used so that one does not have to account for the resistance of the wire leads. The temperature value corresponding to the resistance of the sensor is tabulated in the DIN description number 43760 /32/ and follow the following formula:

$$R_t = R_o \, (1 + \alpha \cdot \theta + \beta \theta^2) \qquad (2)$$

valid in the temperature range from 0 to 850 ^{o}C, where R_t is the resistance in Ω at the temperature t, t is the temperature in ^{o}C and the constants are $\alpha = 3.90802 \cdot 10^{-3}$ deg^{-1}, $\beta = 0.580195 \cdot 10^{-6}$ deg^{-2} and $R_o = 100\Omega$, which is the resistance of the PT 100 sensors at 0 ^{o}C (500 Ω for PT 500).

Neglecting the square term in equ. (2) one gets in the linear approximation for the temperature

$$\theta_L = \frac{1}{\alpha} \left(\frac{R_t}{R_o} - 1 \right) \qquad (3)$$

Using equ. (3) in (2) one gets the expression

$$\theta = \frac{\theta_L}{1 + \frac{\beta}{\alpha} \theta_L} \qquad (4)$$

This rather simple relation is a very good approximation to the exact DIN-formula (2), as shown in /33/. The difference evaluated by equ. (4) to the exact formula equ. (2) is, at t = 65 ^{o}C, only $\Delta t = 1.7 \cdot 10^{-3}$ ^{o}C and at lower

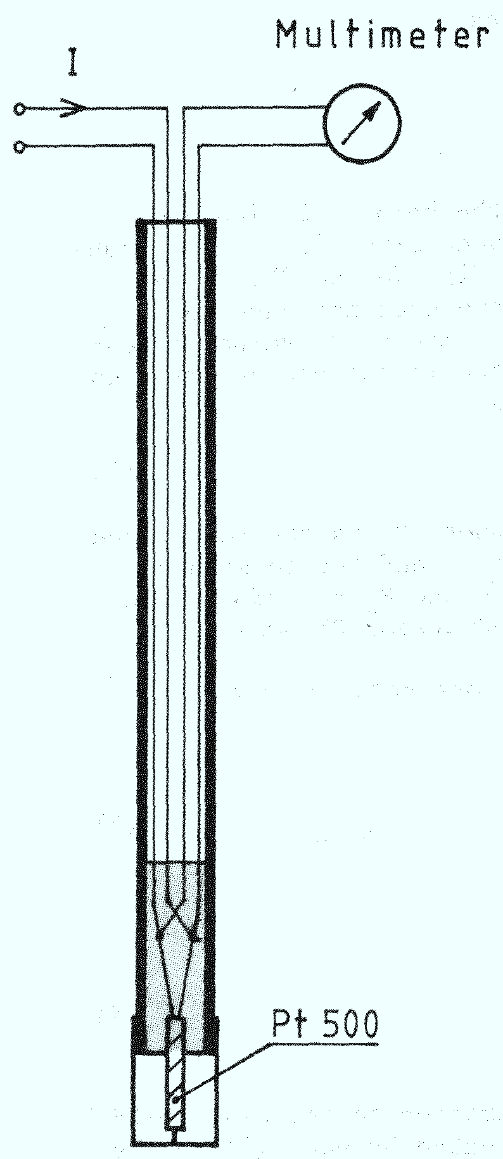

Fig.7a: Arrangement for temperature sensor (PT 500)

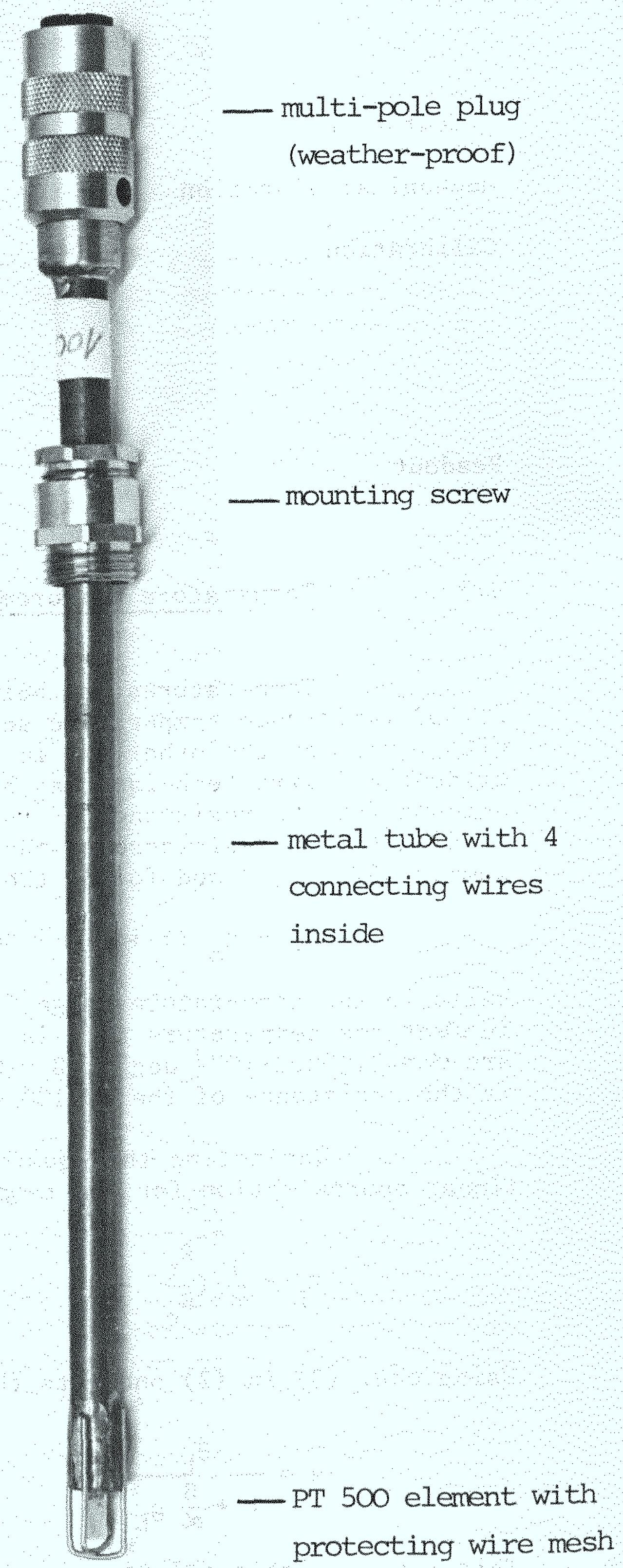

Fig.7b: Photograph of the used PT 500 assembly

temperatures even less. Equ. (4) was used for calculating the temperatures of our experiment via the MADAS data processing system (see section 3.8).

The maximum deviation of the DIN temperature sensors PT 100 and PT 500 up to 60 ^{o}C is ± 0.6 ^{o}C, at lower temperatures less ($\Delta t = \pm(0.3 + 0.05\ |t|)$). For measuring the temperature in 4-wire technique a constant current of 1 mA is sent through the sensor in place (2 wires) and the voltage drop across its resistance R_t is measured with the remaining two wires giving thus the resistance of R_t at temperature t. The change in resistance of the PT 100 sensor with the temperature is 0.39 - 0.38Ω/deg (approx. 2.5 degrees per Ω) in the temperature range 0 ^{o}C - 60 ^{o}C (approx. 1.95Ω/deg or 0.51 deg/Ω for PT 500).

The advantage of using PT 500 instead of the common PT 100 is obviously the higher voltage drop (approx. 550 mV) and the higher change in voltage due to the temperature change, resulting in a better measuring accuracy. A certain disadvantage may be, that the constant current sources (1 mA) must be capable of providing a higher voltage, if a large number of PT 500 are used in series.

- Temperature Measurements in the Collector -

The inlet and outlet tempratures are measured by fixing the sensors at the respective ends of the collector. At the outlet it is expected that a temperature stratification occurs. The sensors are therefore so adjusted as to measure a temperature profile. Five sensors are fixed at the outlet while three sensors are fixed at the inlet. An effort was also made to mix the air at the outlet by making an arrangement so that the upper layers of the air flow to the bottom side and the lower layers flow to the upper side. The temperature distribution along the length of the collector was also measured by putting five temperature sensors between the inlet and the outlet approximately at equal distances from each other. The distribution of the temperature was measured above as well as below the absorber surface (see Fig. 4).

3.6 Relative Humidity Measurements

To get the relative humidity we measured the ambient temperature using a dry bulb and also a wet bulb sensor which are then used for the calculation of the relative humidity from the formula (8). For the ambient temperature the dry bulb temperature of the system was taken. The ambient temperature sensor is housed in a well ventilated instrumentation shelter with its bottom 1.25 m from the terrace and with its door facing north, so that the sun's direct beam does not fall upon the sensor when the door is opened. The instrument shelter is painted white from the outside. Precaution is taken not to have any obstructions higher than twice the height of the house nearby.

Relative humidity of the atmospheric air is calculated from the measurement of dry and wet bulb temperature using the following relations, which are given in /34/. Magnus' formula gives the saturated pressure P_S^*

---

* *For $T_d < 0$ ^{o}C one has to wait with the measurement until the whole wet bulb is frozen and equ. (5) has to be replaced by*

$$P_S(T) = 6.107 \times 10^{\left(\frac{9.5\ T}{265+T}\right)} \qquad (T < 0\ ^{o}C)$$

in mbar as a function of the dry bulb temperature T_d in ^oC for $T_d > 0\ ^oC$.

$$P_S(T_d) = 6{\cdot}107 \times 10^{\left(\frac{7.5\ Td}{237+Td}\right)} \qquad (5)$$

The real vapour pressure is given by Sprung's formula for the ideal psychrometer as a function of the dry (T_d) and wet bulb (T_w) temperatures and the atmospheric pressure P_A

$$P_V = P_S(T_W) - \frac{P_A \cdot C_P}{0.622 \cdot L_V} \cdot (T_d - T_W), \qquad (6)$$

where C_P is the specific heat for dry air, L_V is the heat of evaporation for water and $P_S(T_W)$ is found by replacing T_d by T_W in equ. (5) (0.622 is the ratio of the mol-masses of water and air m_w/m_{air}).

The constant before the psychrometric temperature difference $(T_d - T_W)$ in equ. (6) has the value of 0.492 for P_A = 755 Torr and L_V = 592 cal/g, valid for 10 ^oC. By convention one takes the constant as 0.5 without looking at the change of L_V with temperature.

The relative humidity r as function of the measured dry bulb T_d and wet bulb temperature T_W is given as the quotient of equ. (6) and (5).

$$r = \frac{P_V}{P_S(T_d)} \qquad (7)$$

i.e.

$$r = \frac{P_S(T_W) - 0.5\ (T_d - T_W)}{P_S(T_d)} \qquad (8)$$

Equ. (8) has been used for calculating the instantaneous relative humidity of the ambient air blown through the collector.

The specific heat of the humid air also changes and can be expressed according to /35/ as

$$C_P(T) = C_{Pd}(T) + W(T) \cdot C_{Pm}(T) \qquad (9)$$

where C_{Pd} is the specific heat for dry air and C_{Pm} of moisture, which can be taken from tables.

The humidity W in (9) is given by

$$W = 0.622 \cdot r \cdot \frac{P_S(T)}{P_1 - P_S(T)} \qquad (10)$$

where r is the relative humidity from equ. (8), $P_S(T)$ is the saturated vapour pressure at temperature T and P_1 is the atmospheric pressure.

All the quantities in equ. (9) show a small variation with temperature in the considered temperature range (10 ^oC - 65 ^oC), the effect on the performance data of the collector will be discussed in section 6.

3.7 Wind Speed Measurements

The wind speed was measured almost at the same altitude as the collector test stand with the help of an electronic anemometer obtained from the firm Thies /36/. The instrument gives a DC-voltage in the mV-range and was calibrated in a wind channel. The experimentally formed relation between wind speed v and DC-voltage U is given by the formula /37/

$$v = 0.639 \frac{m}{s} + 0.04119 \frac{m/s}{mV} \cdot U \qquad (11)$$

The smallest voltage difference recorded by the digital voltmeter is 0.1 mV. The constant of 0.639 m/s in equ. (11) is due to some turning losses in the mechanism of the anemometers. The instrument can be used for measuring instantaneous wind speeds in the range of 0.65 - 35 m/sec.

3.8 Data Processing System

In every experiment of thermal application of solar energy the solar radiation data, temperatures, heat fluxes and other weather data have to be measured. These physical quantities are measured by sensors producing a voltage or are characterized by a resistance. As the quantities are all changing slowly with time (time constants are in the region of a second) one can use electronic systems with a low time solution, but having a high accuracy converting the signal into digital values.

The typical voltage values for a solar measuring system will be $U > 100\ \mu V$, the time constants of the sensors will be in the range of $\tau > 100$ msec, and the measuring range will be $\gg$ 1:1000. Then the measurement values can be recorded electronically by an analog-digital converter (ADC) with a 12 bit solution (1:4096) and a voltage solution of about 100 μV. The temperature measurement with a resistance thermometer (PT 100), for instance, are then performed with an accuracy of about 0.2 ^{o}K.

The measurement signals from the different sources are processed by the Microprocessor Aided Data Acquisition System (MADAS) designed and constructed for the different requirements of meteorological collector and system studies /38/.

The MADAS-System, shown in Fig. 8a + 8b is based on the CAMAC standard, which is a convention for a standard communication between different modules and providing a standard power supply to the modules. The main component of the system is the MACAMAC (Micro Autonomous Computer Applied to Measurement And Control), an autonomous Crate Controller equipped with a 8080 INTEL Microprocessor. The controller has an autonomous operation system and uses the BASIC language.

A battery buffered clock is used for controlling the internal system functions. Sensors providing analog signals are connected to the analog/digital converter (ADC). The ADC has 32 channels, and in build scanning system, programmable sensitivity and a constant current source for passive sensors. The scanning rate is about 3 sec/32 channels. The working of the ADCs is based on the dual slope principal by which noise signals are extensively suppressed. Sensors providing pulsed signals (as flow meters) can be connected to the counter. Controlled by the clock the

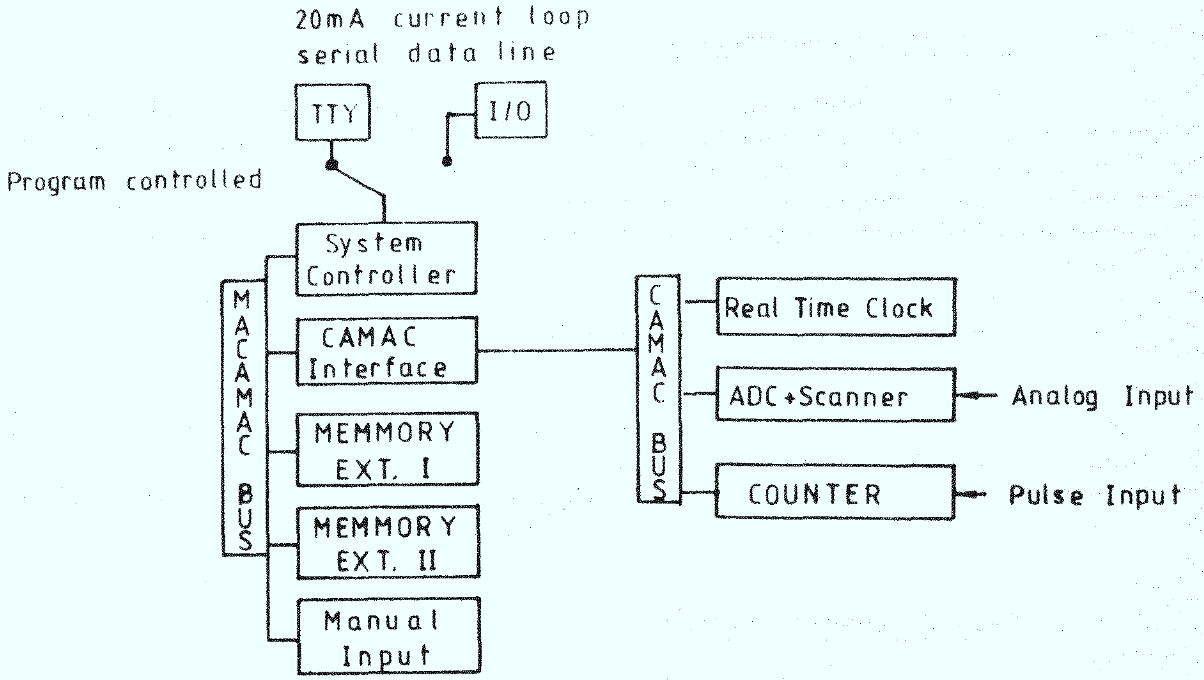

Fig. 8a: The MADAS data processing system

data are shifted to the memory part of the system where they are submitted to the combining and averaging procedure before storage in the internal memory of the system. For our purpose, the system was used together with a HP-Terminal (Hewlett Packard type 2648) where the Basic Programme and the data could be displayed.

In our experiment we used a pyranometer, a wind speed meter and various temperature sensors for the dry and wet bulb temperature (rel. humidity), for the temperature profile at the inlet and outlet of the collector's cross-section, and for the temperature distribution along the length of collector. All instruments deliver analogous DC levels which are fed into the ADC. The data recording and storage is controlled by BASIC programme. The programme calculates iteratively 10 min mean values and variances of all observed quantities which together with time and date are written on a magnetic tape cassette and simultaneously displayed on the terminal.

The pressure drop Δp across the nozzle and the static pressure is read from a Betz manometer and fed into the programme via the terminal manually. The programme calculates the air density ρ as a function of the inlet air temperature and the static pressure (see equ. (32) and then uses Δp and ρ for evaluating the air mass flow $\dot{m}$ (see equ. (1)). From the 10 min (or longer) mean values of the inlet and outlet temperature sensors $\dot{m}$ which is kept constant for longer time intervals and C_p (assumed a constant) and the mean value of the solar radiation the collector efficiency valid for the time interval (usually 10 min) is calculated (see equ. (12)).

4 PERFORMANCE EQUATIONS

Thermal efficiency of a solar collector is usually defined as

$$\eta = \frac{\text{actual useful energy collected}}{\text{solar energy incident/intercepted by the collector}}$$

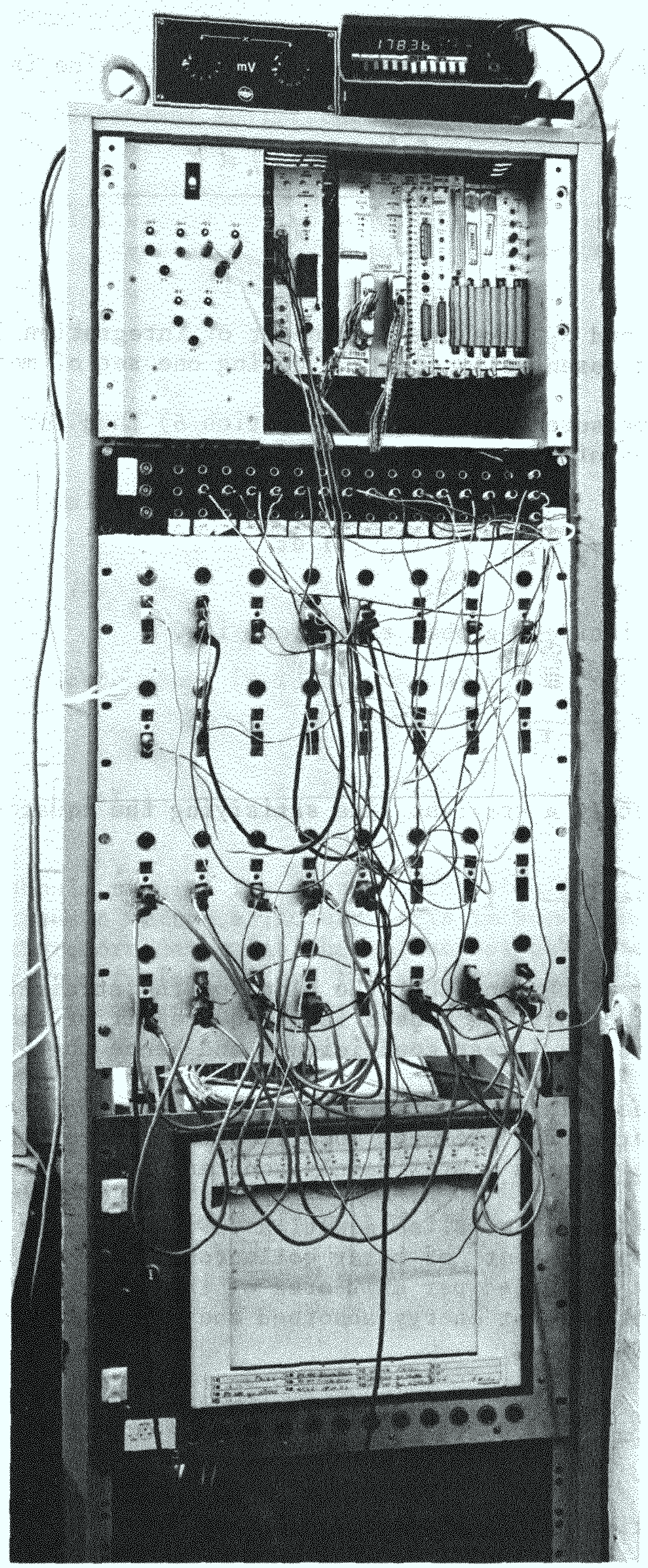

Fig. 8b: The MADAS-System with plug board and cables from the air collector and meteorological instruments. At the bottom is a built in Polycomb recorder.

For each 10 minute segment for which an efficiency value is to be determined, the value is calculated using the equation

$$\eta = \frac{\dot{m} \cdot c_p \cdot \rho \int_{\tau_1}^{\tau_2} (T_o - T_i)\, d\tau}{A \cdot \int_{\tau_1}^{\tau_2} I\, d\tau} \tag{12}$$

The quantities $\dot{m}$ and C_P have been taken out of integration in the numerator since they remain essentially constant during one set of measurements.

Our measurements show (see section 6) that for a constant flow rate the variation of average temperature rise, i.e.

$$\langle \Delta T \rangle = \frac{1}{(\tau_2 - \tau_1)} \int_{\tau_1}^{\tau_2} (T_0 - T_1)\, d\tau$$

with the average incident global radiation, i.e.

$$\langle I \rangle = \frac{1}{(\tau_2 - \tau_1)} \int_{\tau_1}^{\tau_2} I d\tau,$$

follows approximately a straight line satisfying the equation

$$\langle \Delta T \rangle = \frac{\eta A}{\dot{m} C_P} \langle I \rangle \tag{13}$$

From equ. (13) it is obvious that the slope of the straight line enables to calculate the efficiency. We made a least square fit of the $\langle \Delta T \rangle$ vs. $\langle I \rangle$ measurement to get the linear coefficients and hence the efficiency.

A linear increase of $\langle \Delta T \rangle$ with $\langle I \rangle$ for a constant flow-rate over a day indicates that the heat loss coefficient from the collectors system as a whole remains approximately constant.

Hottel-Whillier-Bliss equation /39, 40/ states the instantaneous performance for an element of solar collector. The equation states that the useful energy collected per unit area of the collector is the difference between the amount of solar energy absorbed and the heat loss to the surroundings. Mathematically

$$\frac{q_u}{A} = I \cdot (\tau \cdot \alpha_a)_e - U_L \cdot (T_p - T_a) \tag{14}$$

Using the definition of the efficiency one can write

$$\eta = (\tau \alpha_a)_e - \frac{U_L}{I} (T_p - T_a) \tag{15}$$

For obtaining the detailed information about the performance of collectors and to prevent the necessity of determining some average plate temperature, it is convenient to introduce a parameter F' as

$$F' = \frac{\text{actual useful energy collected}}{\text{useful energy collected if the entire surface collector were at the average fluid temperature}}$$

Mathematically

$$F' = \frac{q_u}{A\left[(\tau\alpha)_e I - U_L(T_f - T_a)\right]} \tag{16}$$

Introducing F' in equ. (15) one gets

$$\eta = F'\left[(\tau\alpha)_e - \frac{U_L}{I}(T_f - T_a)\right] \tag{17}$$

For the mean fluid temperature it is customary to write $(T_o+T_i)/2$; if one plots η against

$$\frac{1}{I}\left(\frac{T_o+T_i}{2} - T_a\right)$$

a straight line should result. The slope of the straight line is some function of U_L and the intercept on the efficiency axis is some other function of $(\tau\alpha)_e$, one can therefore determine the collectors characteristic parameters, i.e. the heat loss coefficient U_L and the collector efficiency factor F'. It should, however, be noted that an approximation of putting

$$T_f = \frac{T_o+T_i}{2}$$

is not essentially a good one, especially for a porous absorber air heater. This is verified by our measurements on the three collectors (see section 6).

Another form of collector performance equation is generally used /6,8,9/. This form is derived from the definition of the heat removal factor /4/ viz

$$F_R = \frac{\text{useful energy collected}}{\text{useful energy collected if the absorber plate were at the inlet fluid temperature}}$$

Mathematically

$$F_R = \frac{q_u}{A\left[(\tau\alpha)_e I - U_L(T_i - T_a)\right]} \tag{18}$$

Substituting in equ. (14) and rearranging one can write

$$= F_R \left[I(\tau\alpha)_e - U_L \, (T_i - T_a) \right] \tag{19}$$

For solar air heaters with matrix absorbers equ. (19) in this form is definitely valid, but does not lead to a straight line if one plots η against $(T_i - T_a)/I$. This is due to not a very simple form of F_R for such porous plate absorbers.*

5 VARIATION OF AIR DENSITY WITH PRESSURE AND TEMPERATURE**

The density of air changes due to change of pressure and temperature. Following Hammecke et al. /42/ we present below the development of a very accurate formula for determining the air density at a given pressure and temperature. The compressibility Z (p,T) of one molecule of a gas is given by

$$Z = \frac{p \cdot V}{R \cdot T} \tag{20}$$

For $n = \frac{m}{M}$ molecules one gets

$$p \cdot V = Z \cdot \frac{m}{M} \cdot R \cdot T \tag{21}$$

i.e.

$$\rho = \frac{1}{Z} \cdot \frac{p \cdot M}{R \cdot T} \tag{22}$$

Comparing the density $\rho(p,T)$ with the density $\rho(p_o,T_o)$ at normal temperature and pressure one gets

$$\rho \cdot Z = \rho_o \cdot Z_o \cdot \frac{p}{p_o} \cdot \frac{T_o}{T} \tag{23}$$

We write

$$\rho(p,\, T) = \frac{\rho^*(p,T)}{Z(p,T)} \tag{24}$$

where

$$\rho^* = \rho_o \cdot Z_o \cdot \frac{p}{p_o} \cdot \frac{T_o}{T} \tag{25}$$

---

* *The form of Hottel Bliss equation for matrix solar collectors will be discussed in a later communication.*

** *In this section the temperatures are defined in ^oK*

Let $$a\,(p,T) = \frac{1}{Z(p,T)} - 1 \qquad (26)$$

Equ. (24), therefore, becomes

$$\rho = \rho^{*} \cdot (1 + a) \qquad (27)$$

From Reference /43/ one can take Z as a function of pressure and temperature and calculate a from the equation (26). Figures 9a and 9b show (-a) as a function of pressure and temperature. The figures show that a maximum value of a is obtained at a temperature of 650 ^oK. In Fig. 10 we show $F(p,T) = a(p,650^oK) - a(p,T)$ as a function of (650-T). The dependence comes out to be linear. One can write, therefore, for a

$$a = A_0 \left(\frac{p}{p_o}\right)^B \left[1 - D \left|\frac{650-T}{T_0}\right|^C\right] \qquad (28)$$

From Fig. 9a one sees that pressure dependence can be represented by B = 1. Factor A_0 can be determined by putting T = 650, so that equ. (28) gives

$$A_0 = a/(p/p_0) \qquad (29)$$

For the pressure of p = 40 atm $\quad A_0 = -3.88 \times 10^{-4}$.

The temperature exponent C is the slope $d \ln F(p,T)/d \ln|650-T|$. One gets C = 3.4. The factor D comes out to be 0.575. Hence

$$a = -3.88 \times 10^{-4} \left(\frac{p}{p_o}\right) \cdot \left[1 - 0.575 \left|\frac{650-T}{T_0}\right|^{3.4}\right] \qquad (30)$$

Substitution of equ. (24) into equ. (26) one gets

$$\rho = \rho_o \cdot Z_o \cdot \frac{p}{p_o} \cdot \frac{T_o}{T} \;(1+a) \qquad (31)$$

For T_o = 273 ^oK and p_o = 1 atm, one can take ρ_o = 1.29304 kg/m^3 and Z_o = 0.99941 from the tables in /43/. Hence from equ.(30) and (31) one finally gets the following equation for the air density

$$\rho = 1.2923 \frac{p}{p_o} \cdot \frac{T_o}{T} \left[1 - 3.88 \times 10^{-4} \frac{p}{p_o} \cdot \left(1 - 0.575 \left|\frac{650-T}{T_0}\right|^{3.4}\right)\right] \qquad (32)$$

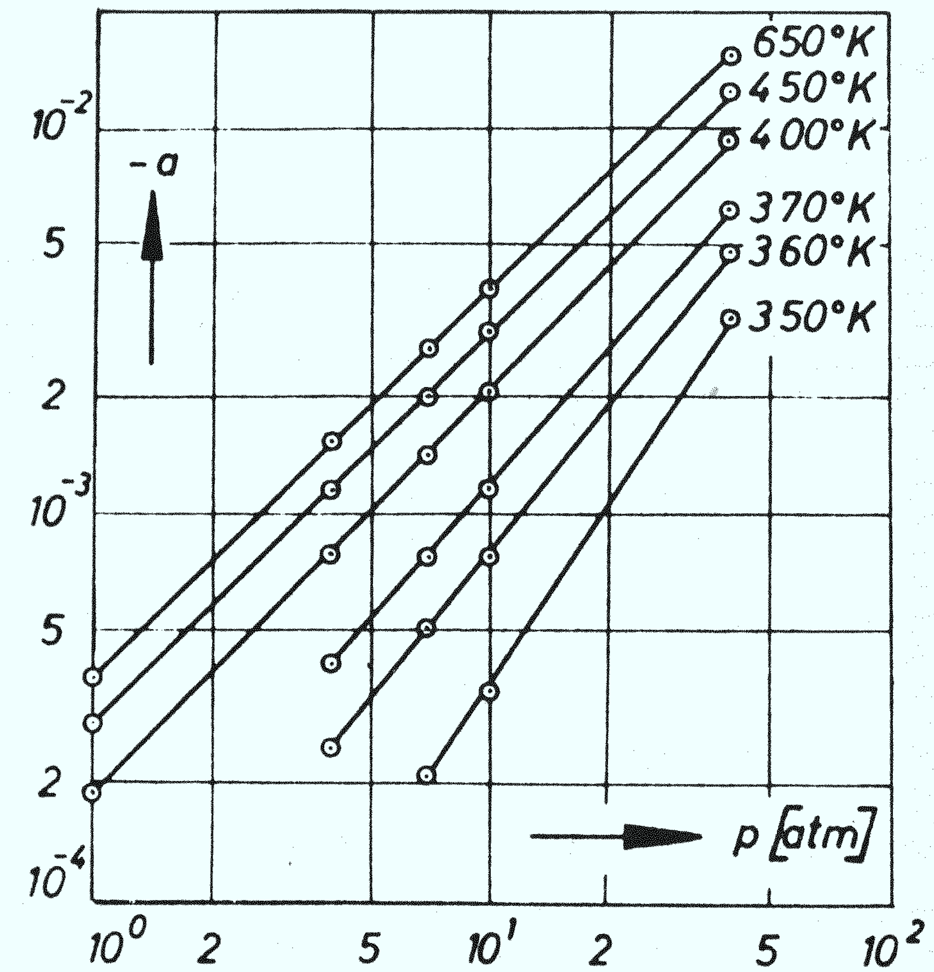

Fig. 9a: Variation of function a with pressure and temperature as parameter

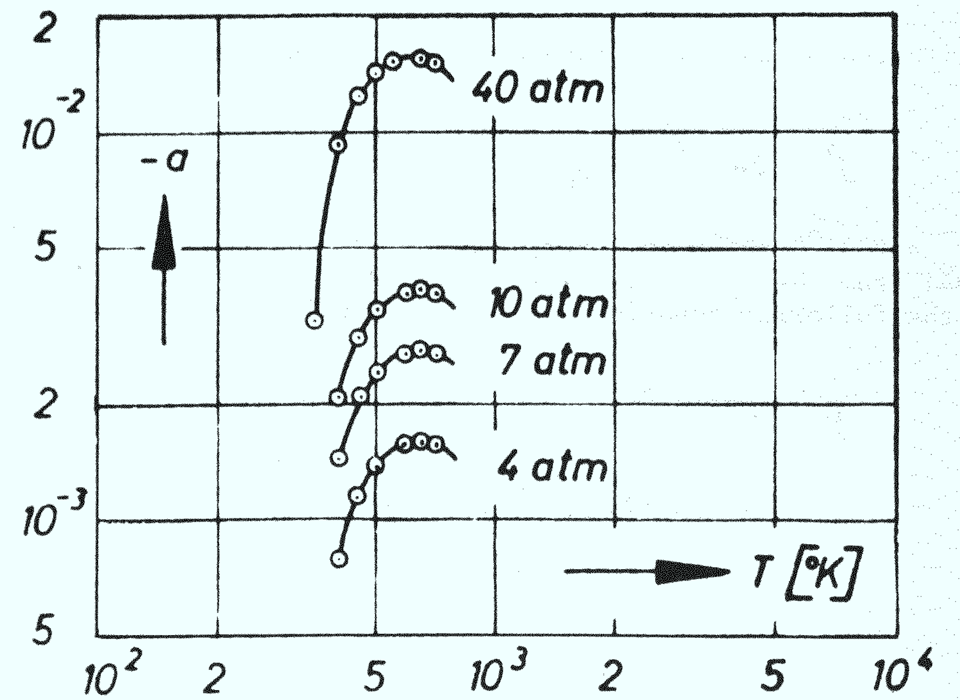

Fig. 9b: Variation of function a with temperature and pressure as parameter

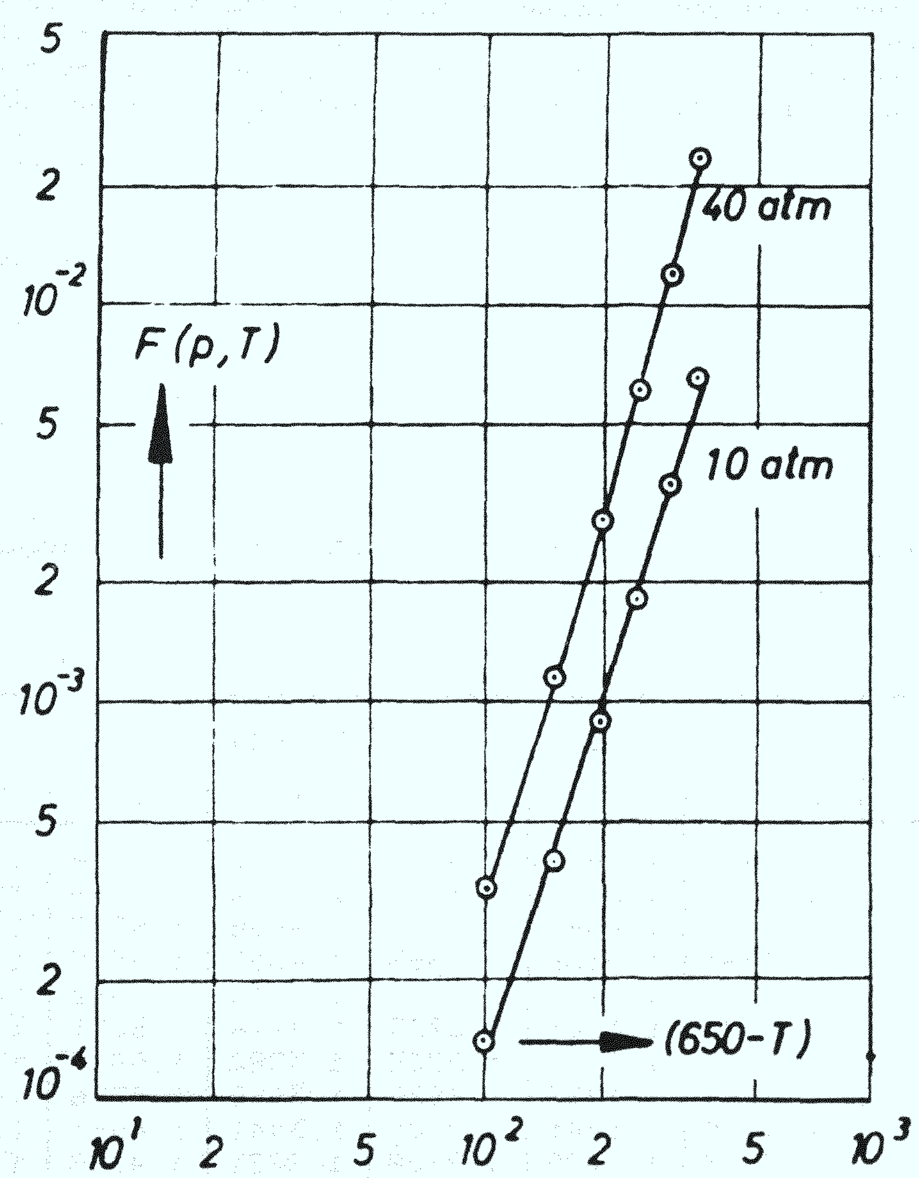

Fig.10: F(p,T) as a function of (650-T) and p as parameter

Equ. (32) was used to calculate the variation in air density in the formula for the output power and efficiency equ. (12) of the solar collectors. The working range is approximately from p = 0.9 atm to 1.11 atm for the static pressure and T = 280 ^{o}K to 340 ^{o}K for the air temperatures. Some typical values of air density at various pressures and temperatures are given in table 2.

Table 2: Variation of air density with temperature and pressure (equ.(32)) in the working range

T [°K]	Density ρ (p,T) in kg/m^3					
	p = 0.9	1.0	1.1	1.2	1.3	1.4 atm
275.0	1.1549	1.2832	1.4116	1.5400	1.6684	1.7967
280.0	1.1342	1.2603	1.3864	1.5124	1.6385	1.7646
285.0	1.1143	1.2381	1.3620	1.4858	1.6097	1.7336
290.0	1.0951	1.2168	1.3385	1.4602	1.5819	1.7036
295.0	1.0765	1.1961	1.3157	1.4354	1.5550	1.6747
300.0	1.0585	1.1761	1.2938	1.4114	1.5291	1.6467
305.0	1.0411	1.1568	1.2725	1.3882	1.5039	1.6196
310.0	1.0243	1.1382	1.2520	1.3658	1.4796	1.5935
315.0	1.0080	1.1201	1.2321	1.3441	1.4561	1.5681
320.0	0.9923	1.1025	1.2128	1.3231	1.4333	1.5436
325.0	0.9770	1.0855	1.1941	1.3027	1.4112	1.5198
330.0	0.9622	1.0691	1.1760	1.2829	1.3898	1.4967
335.0	0.9478	1.0531	1.1584	1.2637	1.3690	1.4743
340.0	0.9338	1.0376	1.1413	1.2451	1.3489	1.4526
345.0	0.9203	1.0225	1.1248	1.2270	1.3293	1.4315
350.0	0.9071	1.0079	1.1087	1.2095	1.3103	1.4110

6 RESULTS AND DISCUSSION

6.1 10 m Collector a

We first put the 10 m collector a for the test. From 28th July 1981 to 24th August 1981 the measurements of the solar intensity were performed on a strip chart recorder and the temperatures were recorded manually with the help of a resistance measuring meter. From 25th August 1981 the data processing system was available for the measurements. The day long measurements of the relevant parameters were performed for various mass flow rates. In Fig. 11 we show one such measurement of various temperatures for a mass flow rate of 371.8 m^3/h. Fig. 12 shows the corresponding variation of the instantaneous efficiency (calculated using equ. (12) over 10 minutes interval). The fluctuations in the outlet temperature, temperature difference and the efficiency correspond to the variations of the solar intensity. While the peaks in the outlet temperature exactly correspond to the peaks in solar intensity curve, the peaks in efficiency are slightly shifted. The reason for this being a certain time constant for the collector. The decrease in temperature of the absorber plate (and hence the outlet temperature) takes place at a slower rate than the decrease in the insolation. A plot of the temperature rise as a function of solar radiation for various air flow rates show that the measurements are scattered around a straight line as shown in Fig. 13. We made a least square fit of the measurements corres-

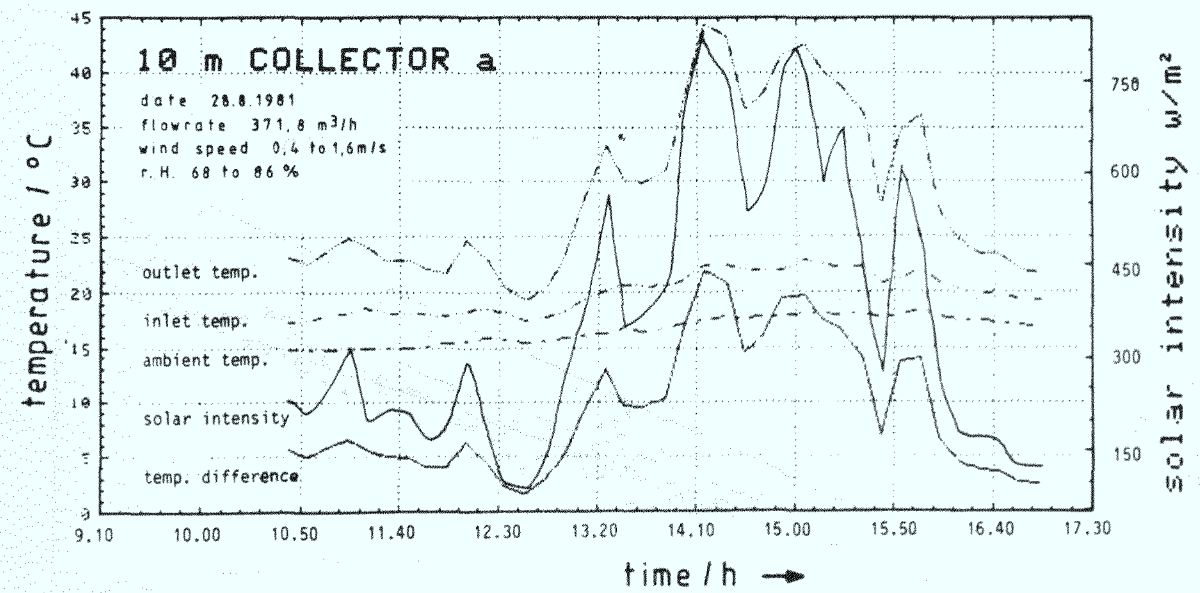

Fig.11: Time variations of various temperatures and solar intentsiy on a typical day

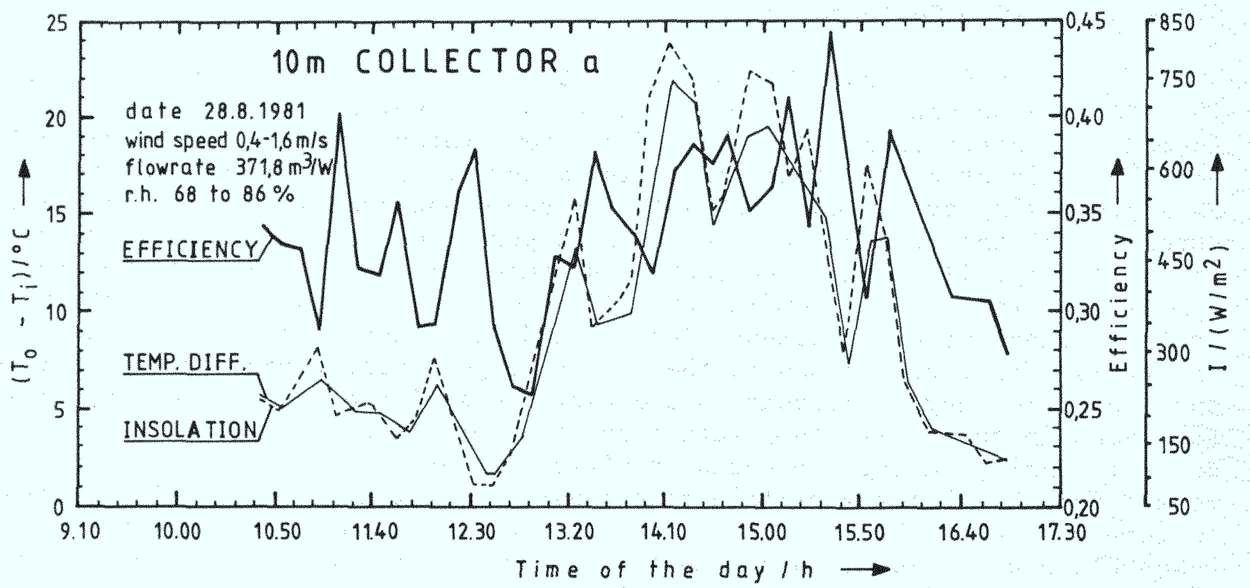

Fig. 12: Time variation of the temperature rise, efficiency and solar intensity on typical day.

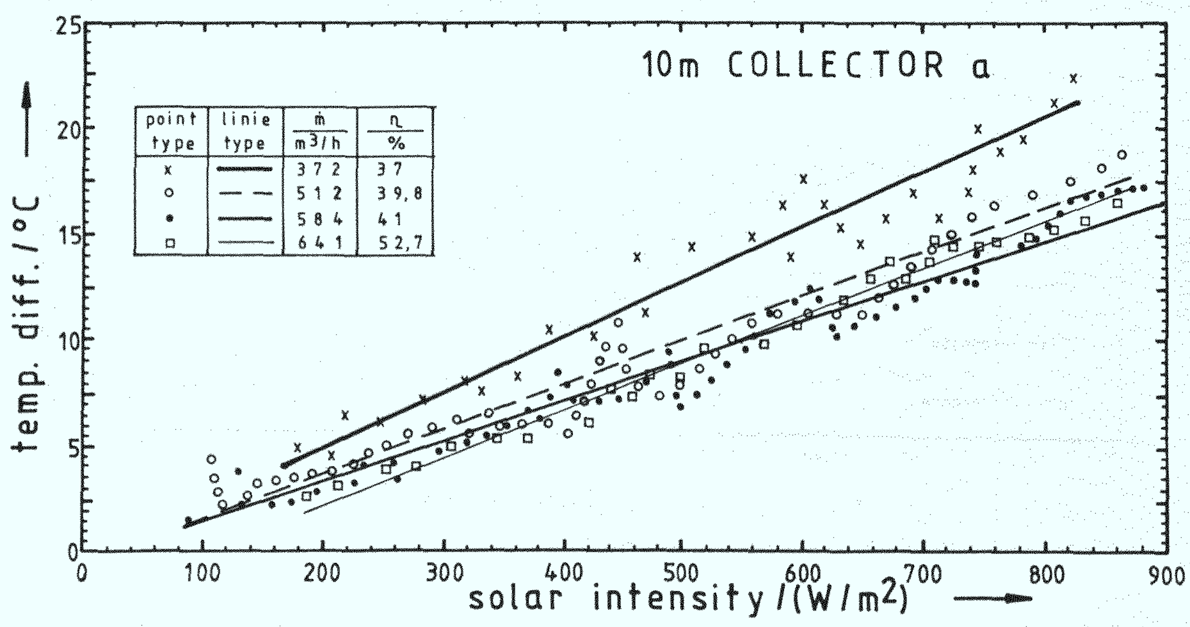

Fig. 13: Variation of temperature rise with solar intensity for various air flow rates

ponding to the appropriate line and back calculated the efficiency from the slope of the appropriate curve (eqn.13). The calculated efficiencies for various flow rates are also tabulated in the same figure 13. Such a curve, as one can see, carries maximum information as it gives for a particular rate of air flow and for a particular intensity, the temperature difference and the efficiency of the collector. The efficiencies may, however, differ from the instantaneous efficiency. In Fig. 14 we have plotted the measurements, over 10 minutes interval, of efficiency and temperature rise performed in almost constant radiation conditions. A dip in the efficiency around flow rates of 660 m^3/h and 700 m^3/h is due to change in the meterological conditions and the related thermal losses. The efficiency and the temperature rise curve show a saturating trend beyond an air flow of 600 m^3/h. A maximum efficiency of around 50 % shown in Fig. 14 is five percent smaller than obtained from the least square fit of Fig. 13. The later, however, contains errors of averaging etc., however the straight line graphs are found to be good from the point of view of comparing the performance of collectors.

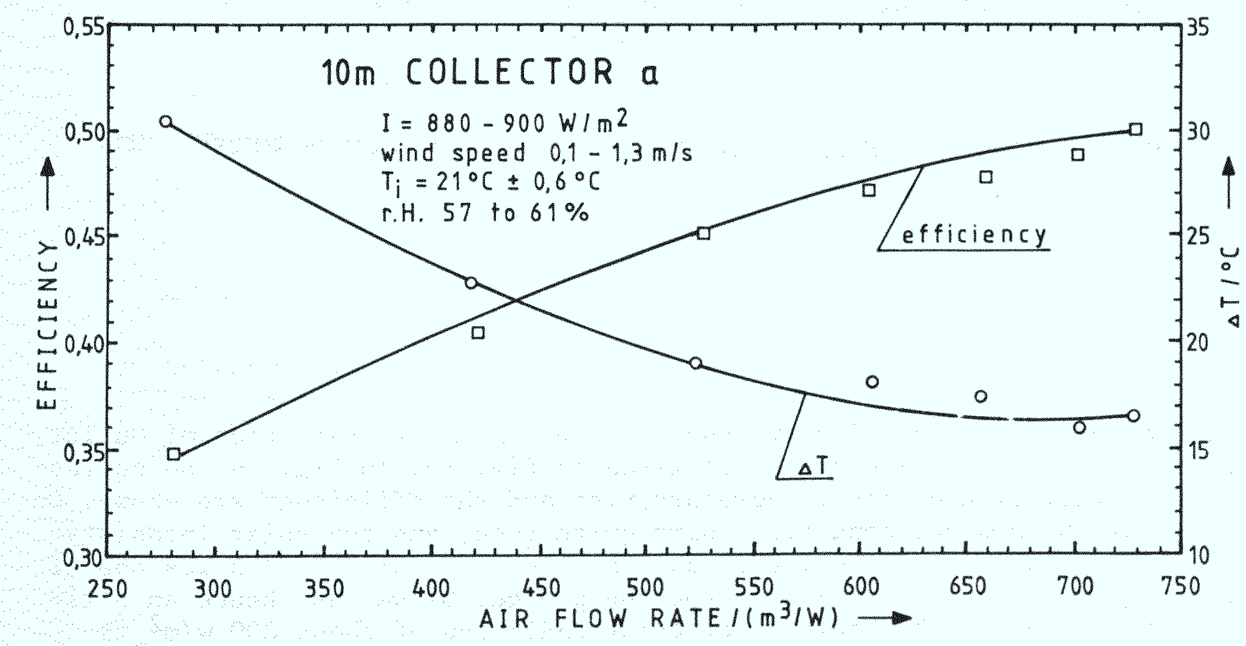

Fig. 14: Variation of efficiency and temperature rise with air flow rate

6.2 10 m Collector b

This collector was tested for a period of one week starting from 2nd September 1981. Each day the flow rate was changed and the measurements

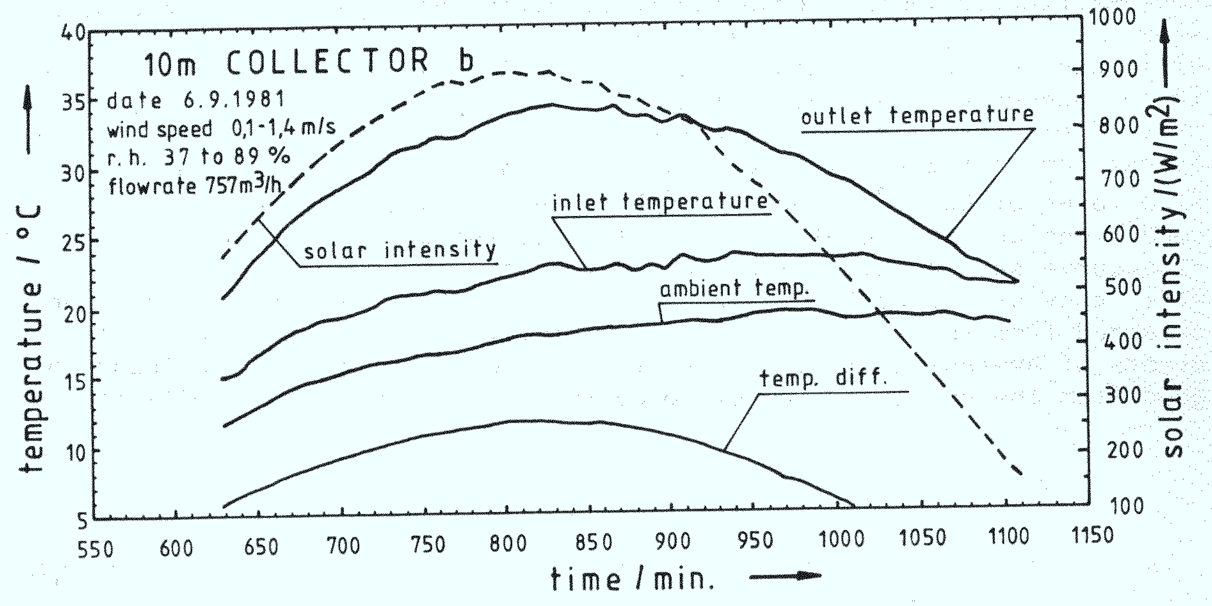

Fig.15: Time variation of solar intensity and various temperatures on a clear day

were recorded. A typical curve showing the ten minute variation of outlet, inlet and ambient temperatures is given in Fig. 15. In Fig. 16 the corresponding variation of the temperature rise and the efficiency are shown. On this day the ambient conditions were quite good, and the solar intenisty was also constant over long periods. The flow rate of 757 m^3/h was one of the highest one could achieve from the present blower and hence an efficiency of about 32 % obtained for solar radiation of about 800 w/m^2 is almost the maximum one can obtain from this collector. This efficiency is markedly lower than that obtained from the 10 m collector. The reasons for getting this low efficiency are discussed later in section 6.4.

Measurements of ΔT, the temperature increase for various air flow rates and for various magnitudes of solar intensity are shown in Fig. 17. The measurements were fitted to a straight line by the least square method and from the corresponding slope of the straight line the efficiencies were calculated which are given in Fig. 17. The efficiencies obtained by this method are found to differ with the values of the instantaneous efficiencies measured over ten minutes interval for approximately constant solar radiation. The instantaneous efficiencies are plotted in Fig. 18.

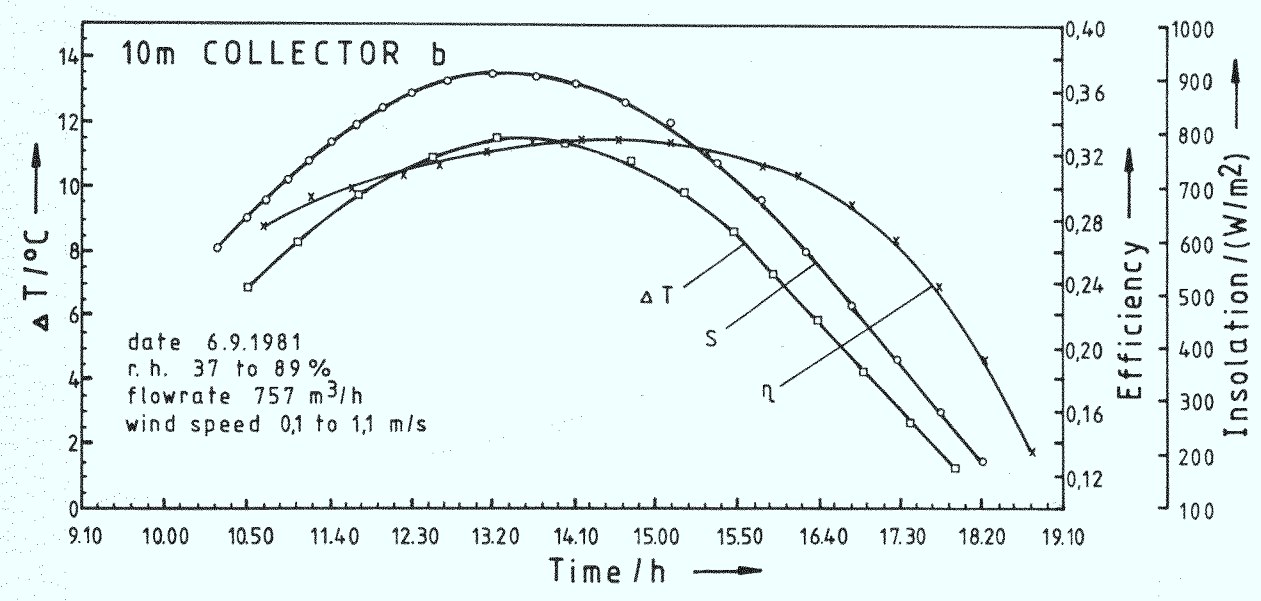

Fig.16: Time variation of solar intensity S, temperature rise ΔT and efficiency η on a clear day.

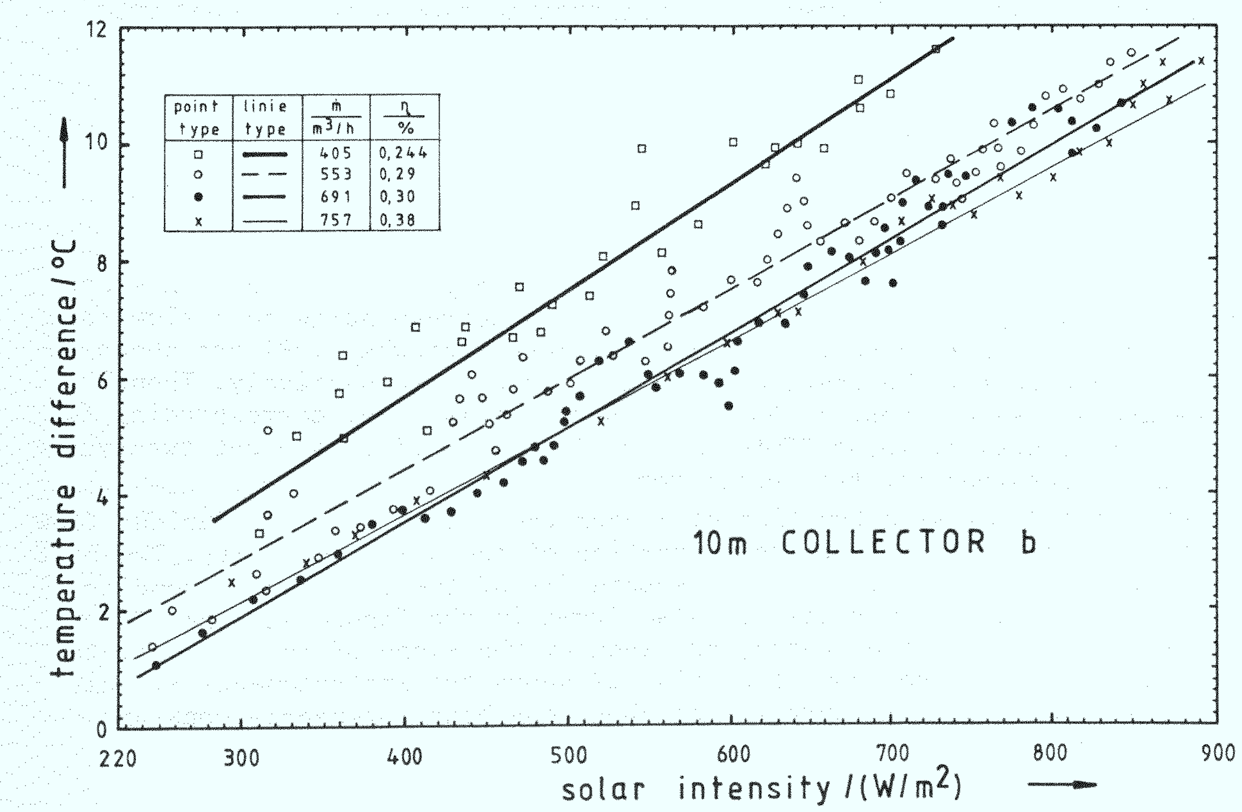

Fig.17: Variation of temperature rise with solar intensity for various air flow rates

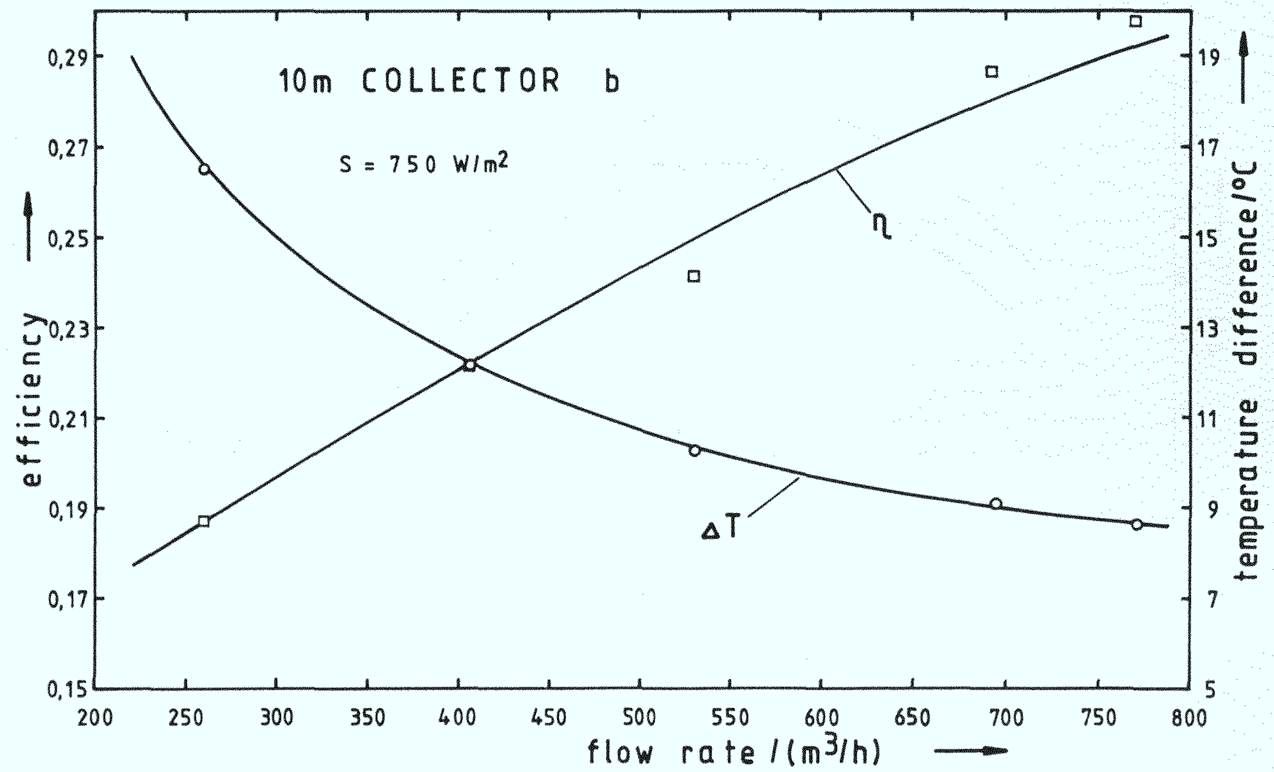

Fig.18: Variation of efficiency and temperature rise with air flow rate

6.3 20 m Collector

This collector was also tested for a period of one week starting from 9th September 1981. The measurements corresponding to a flow rate of 697 m^3/h and for weather conditions of 10th September 1981 are shown in Figs. 19 and 20 for the temperature and efficiency respectively. Though a temperature rise of about 17 ^oC is reached in this case, corresponding to a solar intensity of about 850 w/m^2, an efficiency of only about twentynine percent is obtained for this collector.

Measurements of ΔT as a function of I over the entire days for various flow rates are plotted in Fig. 21 as a function of the solar intensity. The best fit lines obtained through a least square fit of the data, corresponding to the appropriate flow rates are also drawn in the figure and the efficiencies for various flow rates, as given by the slope of the appropriate straight line are also tabulated. Fig. 22 shows the instantaneous efficiency measured over a small duration of about one hour for nearly constant intensity of $\sim$ 850 w/m^2.

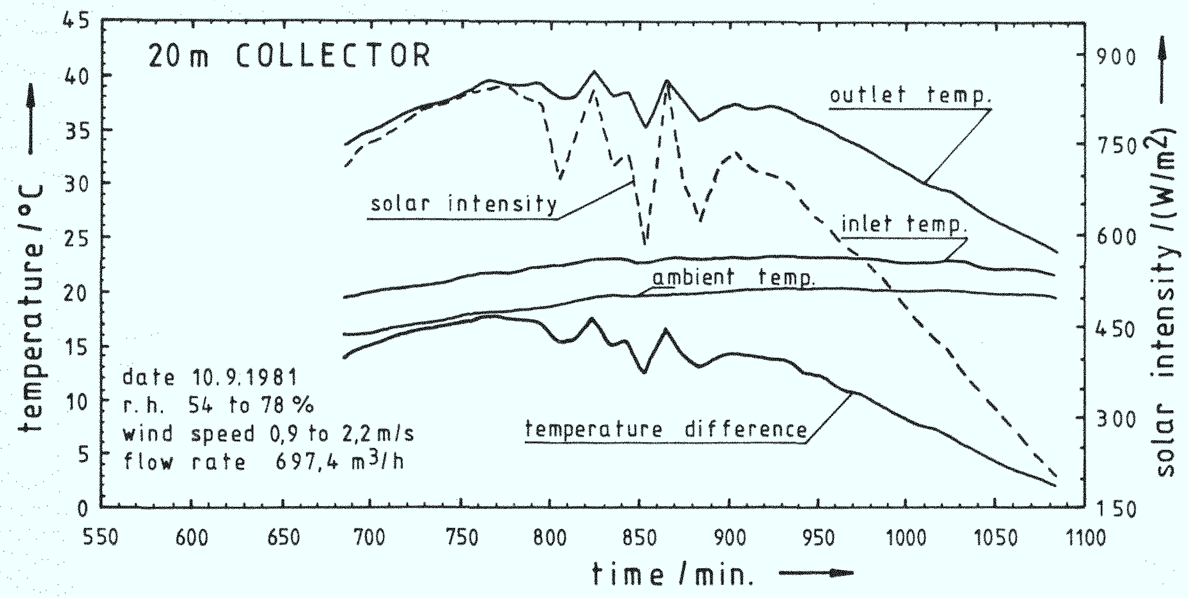

Fig.19: Time variation of various temperatures and solar intensity on a typical day

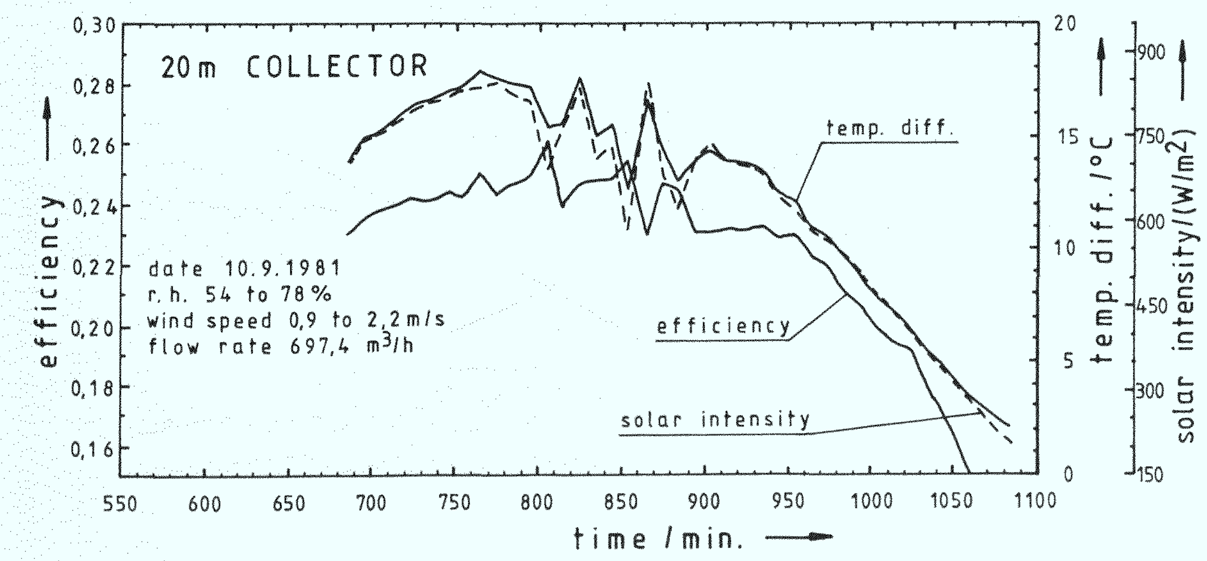

Fig.20: Time variation of efficiency, temperature rise and solar intensity on a typical day

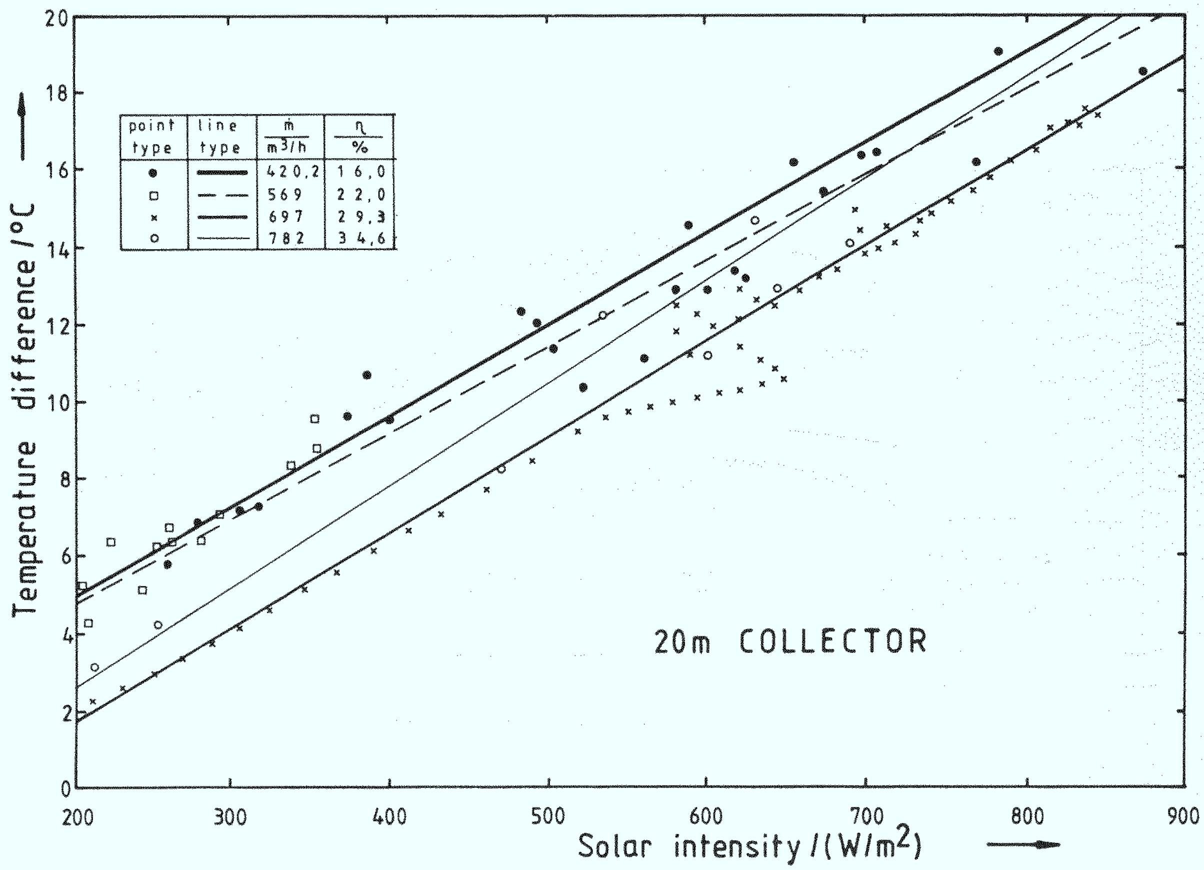

Fig.21: Variation of temperature rise with solar intensity

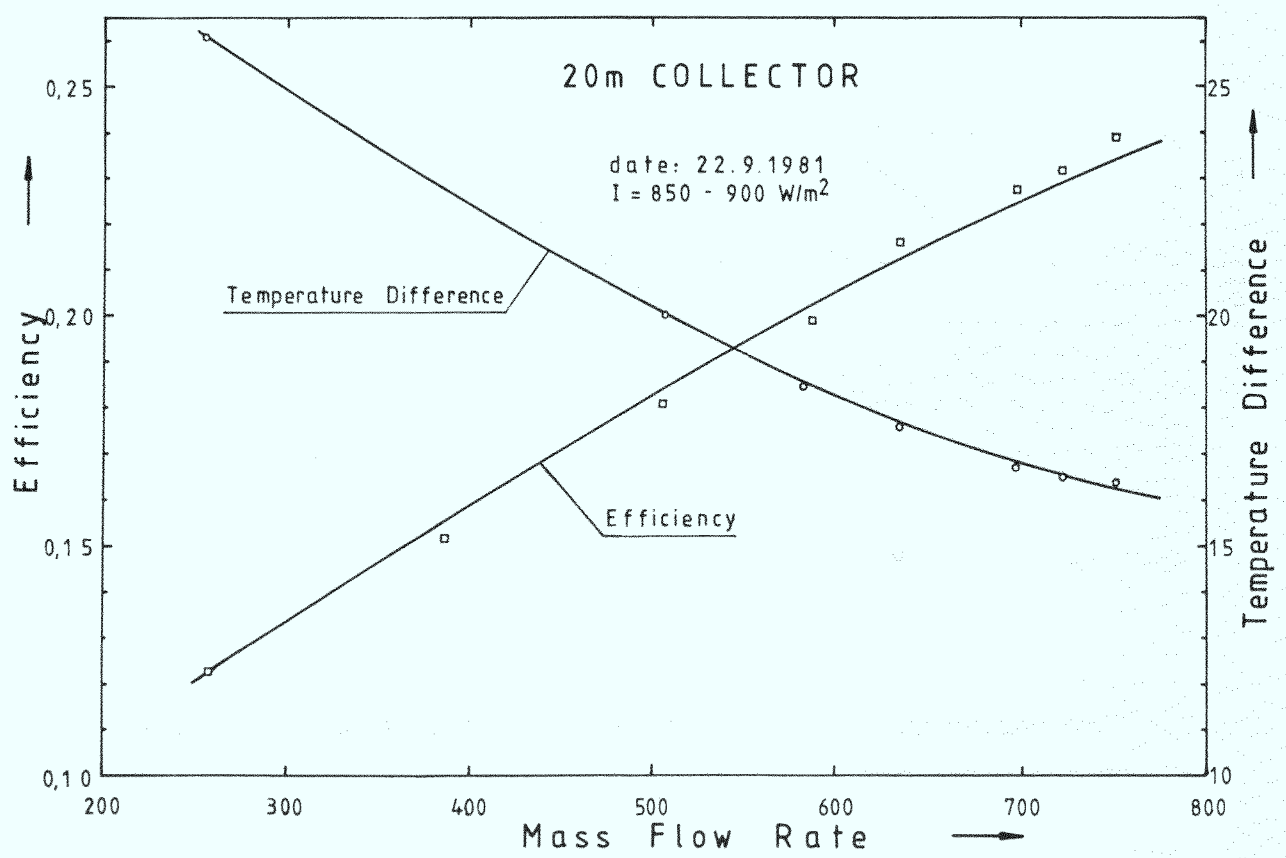

Fig.22: Variation of efficiency and temperature rise with air flow rate

6.4 Comparison of the Collectors

A comparison of the temperatures of the flowing air at the outlet, temperature rise obtained in the collectors for various flow rates and the instantaneous (equ. (12)) efficiency of the three collectors for various air flow rates is tabulated in table 3. It is easily seen from the table that the performance of 10 m collector a is much better than the performances of either 10 m collector b or the 20 m collector. The efficiency of 10 m collector a is almost double than that of 10 m collector b. The efficiency of 20 m collector is still low. Even the temperature rise obtained from the 10 m collector a is more than that obtained by 20 m collector up to an air flow rate of 410 m^3/h after which it is almost equal to the temperature rise obtained in the 20 m collector. The efficiency of 20 m collector is seen to be less than the efficiency of 10 m collector b having the same textile. This is because the temperature rise is not in proportion to the increase in area. Due to increase in the area of the collector, thermal losses also become more (radiative losses not being linear). It is also noted that the efficiencies calculated by least square fitting the ΔT versus I (Figs. 13, 17, 21) also differ in the same proportion for these collectors. Increasing flow rates results in increasing fan power as evident from the last but one column of table 3. This consumed electrical power should be subtracted from the thermal power $q_u = \eta \cdot I \cdot A$ to get the useful power. This is also given in table 3. It should be noted that though q_u goes on increasing with the flow rate in an approximately exponential manner, the useful power Q_u is maximum at a particular flow rate.

The reason for the difference in the performances of various collectors is essentially due to two reasons:

(1) Due to the difference in the absorptance of the black absorber tissue,

(2) Due to the different density of pores in the two absorbers.

Table 3: Comparison of the thermal performance of the three collectors

S.N.	I w/m^2	$\dot{m}$ m^2/h	T_i °C			T_o °C			ΔT °C			η %			Q_{th} W			Pel.W	Q_u		
			$10m^a$	$10m^b$	20m	$10m^a$	$10m^b$	20m	$10m^a$	$10m^b$	20m	$10m^a$	$10m^b$	20m	$10m^a$	$10m^b$	20m		$10m^a$	$10m^b$	20m
1	900	730	20.3	20.1	20.2	36.6	29.9	37.0	16.3	9.8	16.8	48.3	26.5	22.7	3966	2383	4086	363	3603	2020	3723
2	900	700	20.4	21.7	19.9	37.3	31.8	37.4	16.9	10.1	17.5	48.0	26.2	22.6	3942	2356	4082	326	3616	2030	3756
3	900	660	20.8	22.6	18.7	38.2	33.1	36.9	17.4	10.5	18.2	46.6	25.7	22.2	3826	2310	4001	299	3527	2011	3702
4	900	610	21.2	21.6	19.5	39.4	32.6	38.2	18.2	11.0	18.7	45.1	24.8	21.1	3698	2237	3798	245	3453	1992	3553
5	900	520	21.8	21.7	18.7	41.2	33.3	38.8	19.4	11.6	20.1	40.9	22.3	19.3	3557	2009	3481	220	3137	1789	3261
6	900	410	21.7	21.7	20.0	45.9	33.9	40.6	23.4	12.2	20.6	38.9	18.5	15.6	3195	1665	2813	164	3031	1501	2649
7	900	270	20.1	21.9	21.9	50.6	39.8	48.0	30.5	17.9	26.1	33.4	17.8	13.0	2742	1602	2345	112	2630	1490	2233

The absorptance of the textile absorber (Fig. 3a) used in 10 m collector a is fifteen percent more than the absorptance of the textile absorber (Fig. 3b) used in the collector 10 m collector b or 20 m collector. This increase in the absorptance is, however, not able to explain rather big difference in the efficiencies of the collectors with the two textiles. In Fig. 23 we have plotted the temperature profiles measured along the length of the collectors, above as well as below the textile absorbers. Above the black textile, the temperature is seen to be increasing steadily along the length in the 10 collector b and the 20 m collector. In the 10 m collector a the temperature of the air above the absorber is nearly equal to ambient (except at very small rates of air flow). The thermal losses in the 10 m collector a from the top are therefore much less than the other two collectors. Moreover, Fig. 3b shows that this textile is denser than the textile whose surface photograph is given in Fig. 3a. In 10 m collector b and also in 20 m collector all the air is not able to go through the textile and builds a pressure at the outlet end of the collector. This is also born out from a study of the temperature variation (along the length of the collector) below the textile absorber in both the 10 m collector and the 20 m collector. The temperature is seen to be increasing with the length till the outlet end (for 10 m collector b) and suddenly dropping down due to increased air flow from the top of the absorber to the outlet. In the 20 m collector the maximum of the temperature is seen to be reached around a distance of 15 m from the inlet and then decreasing. In the 10 m collector a, the temperature variation (along length) shows a fluctuating behaviour; the reason being the nonuniform porousity of the porous absorber as evident from Fig. 3b. A better absorption of solar radiation and better porosity of the textile absorber of 10 m collector a are thus responsible for its good thermal performance.

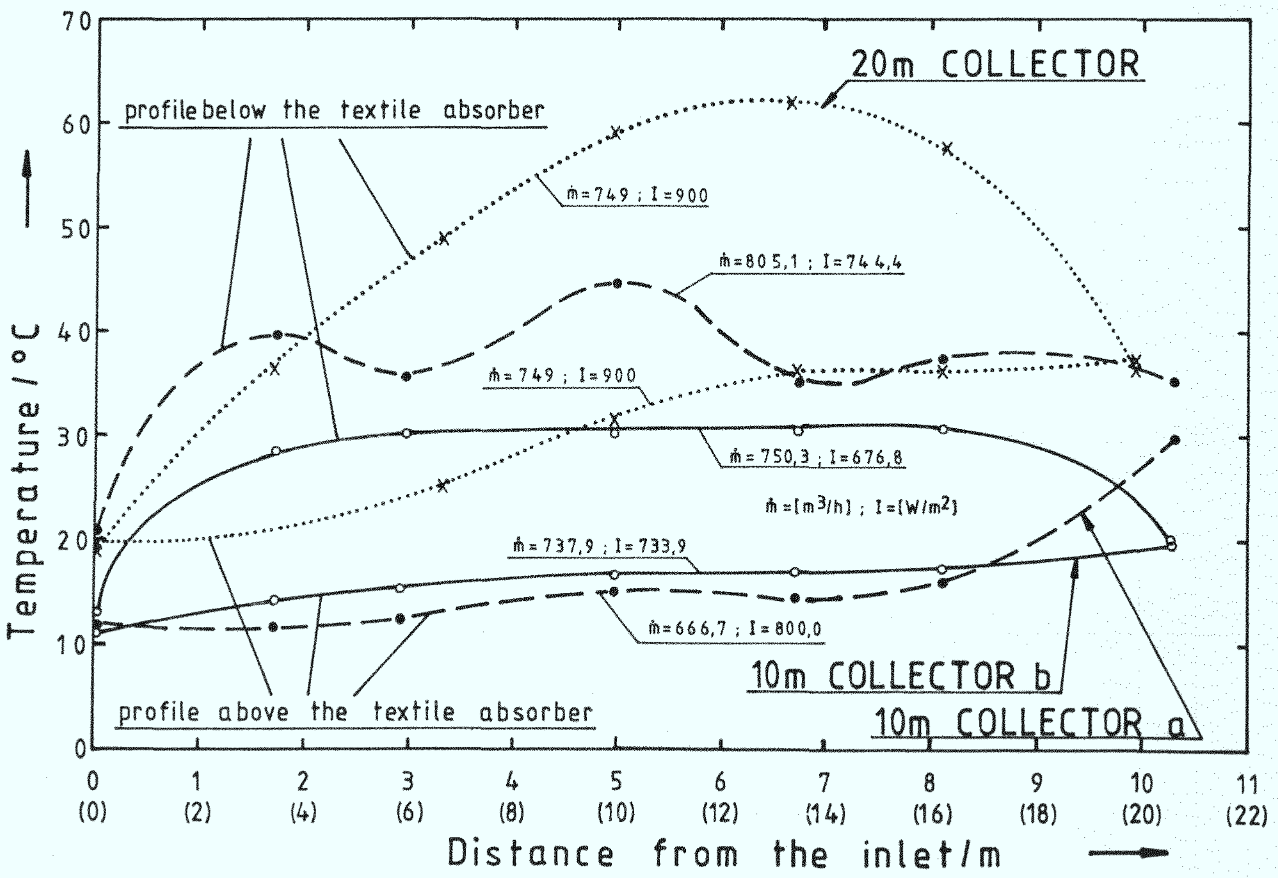

Fig. 23: Temperature profile in the collectors along length

6.5 Effect of Back Insulation

The insulation at the back of the collector improves the efficiency of the collector especially that of 10 m collector a. This effect was studied in two steps. First we put a simple aluminium foil above the 3 cm thick polyethylene insulation (which was at the back of the collector in all the previously described measurements) and measured the average

Table 4: Performance of 10 m collector a with and without aluminium foil over the back insulation for incident solar intensity of 700 W/m^2.

S.N.	$\dot{m}$ m^3/h	ΔT °C I	ΔT °C II	η % I	η % II
1	372	16.8	22.5	32	44
2	511	16.0	20.5	41	57
3	583.7	14.0	18.0	43	58
4	657.2	14.5	18.4	46	59

I Polyethylene as back insulation

II Polyethylene with an aluminium foil as back insulation

temperature rise of the air flowing at different rates over ten minutes interval. Typical measurements along with the calculated efficiencies are summarised in table 4 along with the corresponding measurements performed without the aluminium foil. For all the flow rates the efficiencies recorded with an aluminium foil show a remarkable improvement. The unexpected result of relatively less increase in the efficiency for the lowest flowrate, i.e. 372 m^3/h, in comparison to higher flowrates is due to the increasing thermal losses through the cover for smaller flow rates. In fact for still smaller flow rate ($\sim$ 270 m^3/h) the efficiency observed with aluminium foil was even lower than the efficiency without aluminium foil due to a much colder day in the former case. For very small flow rates the air keeps mainly on the upperside of the absorber and is not able to flow through the pores effectively. We notice not much improvement in the efficiency of 10 m collector b under similar conditions due to the same reason.

Though Fig. 2 shows a rather low transmittance of the PVC foil in the temperature of interest, yet to make sure that the improvement in the thermal performance of the 10 m collector a is not due to the reflections of IR radiation, which might come through the back PVC foil, we placed a 6 cm thick polyethylene insulation below the collector and carried out the measurements which are given in table 5. A remarkable result of obtaining as high an efficiency as 70.6 percent is achieved for an air flowrate of about 800 m^3/h. Considering the simplicity and low cost of the collector the result is really very encouraging. From table 5 also one notices a comparatively lower efficiency for the lowest flow rate. The reason for this again being the same as discussed earlier, i.e. sticking of air over the upper surface of the absorber for low flowrate and hence increased thermal losses from the top. It is, therefore, ovious that for such type of collector a threshold or minimum airflow rate $\gtrsim$ 500 m^3/h is desirable.

Table 5: Performance of 10 m collector a with different back insulations (figures in brackets indicate the incident solar radiation in W/m^2 on the collector surface)

S.NO	$\dot{m}$ (m^3/h)	Temperature Rise °C			Efficiency %		
		I	II	III	I	II	III
1	420	23.4 (900)	23.9 (748)	22.8 (732)	0.3991	0.4905	0.4781
2	545	19.4 (836)	18.0 (682)	20.4 (746)	0.4622	0.5257	0.5447
3	645	18.2 (876)	18.4 (800)	19.2 (743)	0.4898	0.5421	0.6090
4	718	17.4 (908)	13.9 (656)	18.8 (752)	0.5029	0.5560	0.6561
5	770	15.9 (855)	13.9 (700)	18.3 (759)	0.5233	0.5588	0.6785

I 3 cm thick polyethylene

II 3 cm thick polyethylene with aluminium foil above it

III 6 cm thick polyethylene

6.6 Pressure Drop in the Collector

A good porous construction of the absorber plate also results in a smaller pressure drop across the collector. The pressure drop, measured by the static pressure difference across the inlet and the outlet, in the 10 m collector a and 10 m collector b as a function of various air flow rates is shown in Fig. 24. As expected the pressure drop across the 10 m collector b, which has the denser absorber textile of Fig. 3b, is much higher (approximately a factor of 2) than the pressure drop across the 10m collector a. In collector a the air is steadily passing through the absorber along the whole length, while in the collector b more air flows along the top up to the end and then passes through the textile to the outlet. Since the air in textile of Fig. 3a passes through it, the heat transfer is from the entire volume resulting in high average ΔT and hence the higher efficiency in comparison to the corresponding performance of the textile of Fig. 3b.

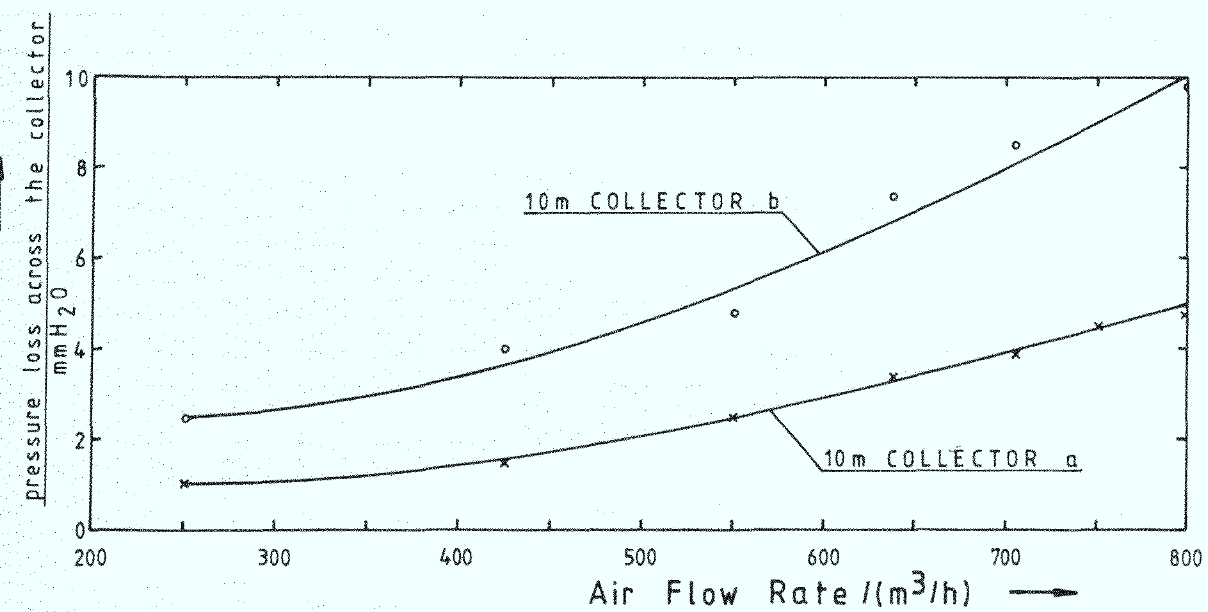

Fig.24: Pressure loss as a function of air flow rate in the two collectors of the same length

6.7 Effect of Relative Humidity on the Thermal Efficiency

Relative humidity of the inlet air affects the thermal efficiency of the solar air heaters through its specific heat, which varies with the amount of water vapour present in the air according to the formula given in equ. (9). Calculated values of C_p at various temperatures and relative humidity are given in table 6; the saturated vapour pressure at various temperatures has been taken from the standard tables /45/. The specific heats C_{Pd} and C_{Pm}

Table 6: Variation in the specific heat of air with relative humidity r and temperature T

T°C \ r	0.30	0.35	0.40	0.45	0.50	0.55	0.60	0.65	0.70	0.75	0.80	0.85	0.90	0.95	1.00
10.0	1.012	1.013	1.014	1.014	1.015	1.016	1.017	1.017	1.018	1.019	1.020	1.020	1.021	1.022	1.022
12.0	1.013	1.014	1.015	1.015	1.016	1.017	1.018	1.019	1.020	1.020	1.021	1.022	1.023	1.024	1.024
14.0	1.014	1.015	1.016	1.016	1.017	1.018	1.019	1.020	1.021	1.022	1.023	1.024	1.025	1.026	1.027
16.0	1.014	1.016	1.017	1.018	1.019	1.020	1.021	1.022	1.023	1.024	1.025	1.026	1.027	1.028	1.029
18.0	1.017	1.019	1.021	1.022	1.024	1.025	1.027	1.028	1.030	1.031	1.033	1.035	1.036	1.038	1.039
20.0	1.016	1.018	1.019	1.021	1.022	1.023	1.025	1.026	1.027	1.029	1.030	1.032	1.033	1.034	1.036
22.0	1.017	1.019	1.021	1.022	1.024	1.025	1.027	1.028	1.030	1.032	1.033	1.035	1.036	1.038	1.039
24.0	1.019	1.021	1.022	1.024	1.026	1.028	1.029	1.031	1.033	1.035	1.037	1.038	1.040	1.042	1.044
26.0	1.020	1.022	1.024	1.026	1.028	1.030	1.032	1.034	1.036	1.038	1.040	1.042	1.044	1.046	1.048
28.0	1.022	1.024	1.026	1.029	1.031	1.033	1.035	1.038	1.040	1.042	1.044	1.047	1.049	1.051	1.054
30.0	1.023	1.026	1.029	1.031	1.034	1.036	1.039	1.041	1.044	1.047	1.049	1.052	1.054	1.057	1.059
32.0	1.025	1.028	1.031	1.034	1.037	1.040	1.043	1.046	1.049	1.051	1.054	1.057	1.060	1.063	1.066
34.0	1.028	1.031	1.034	1.037	1.041	1.044	1.047	1.051	1.054	1.057	1.060	1.064	1.067	1.070	1.073
36.0	1.030	1.034	1.037	1.041	1.045	1.048	1.052	1.056	1.059	1.063	1.067	1.070	1.074	1.078	1.081
38.0	1.033	1.037	1.041	1.045	1.049	1.053	1.057	1.062	1.066	1.070	1.074	1.078	1.082	1.086	1.090
40.0	1.036	1.040	1.045	1.050	1.054	1.059	1.063	1.068	1.073	1.077	1.082	1.087	1.091	1.096	1.100
42.0	1.039	1.044	1.050	1.055	1.060	1.065	1.070	1.075	1.081	1.086	1.091	1.096	1.101	1.106	1.112
44.0	1.043	1.049	1.055	1.060	1.066	1.072	1.078	1.084	1.089	1.095	1.101	1.107	1.113	1.118	1.124
46.0	1.047	1.054	1.060	1.067	1.073	1.080	1.086	1.093	1.099	1.106	1.112	1.119	1.125	1.132	1.138
48.0	1.052	1.059	1.066	1.074	1.081	1.088	1.096	1.103	1.110	1.117	1.125	1.132	1.139	1.147	1.154
50.0	1.057	1.065	1.073	1.082	1.090	1.098	1.106	1.114	1.122	1.130	1.139	1.147	1.155	1.163	1.171
52.0	1.063	1.072	1.081	1.090	1.100	1.109	1.118	1.127	1.136	1.145	1.154	1.163	1.173	1.182	1.191
54.0	1.070	1.080	1.090	1.100	1.111	1.121	1.131	1.141	1.151	1.162	1.172	1.182	1.192	1.203	1.213
56.0	1.077	1.088	1.100	1.111	1.123	1.134	1.146	1.157	1.169	1.180	1.192	1.203	1.215	1.226	1.237
58.0	1.085	1.098	1.111	1.124	1.137	1.150	1.162	1.175	1.188	1.201	1.214	1.227	1.240	1.252	1.265
60.0	1.097	1.112	1.126	1.141	1.156	1.171	1.186	1.200	1.215	1.230	1.245	1.259	1.274	1.289	1.304
62.0	1.105	1.121	1.137	1.153	1.170	1.186	1.202	1.218	1.234	1.250	1.266	1.283	1.299	1.315	1.331
64.0	1.115	1.133	1.151	1.168	1.186	1.204	1.222	1.240	1.257	1.275	1.293	1.311	1.328	1.346	1.364
66.0	1.136	1.157	1.178	1.200	1.221	1.242	1.263	1.285	1.306	1.327	1.348	1.370	1.391	1.412	1.433
68.0	1.150	1.174	1.198	1.221	1.245	1.269	1.292	1.316	1.340	1.363	1.387	1.411	1.434	1.458	1.482
70.0	1.166	1.192	1.218	1.245	1.271	1.297	1.323	1.350	1.376	1.402	1.428	1.455	1.481	1.507	1.533

of dry air and moisture respectively also change with temperature, but the variation being slow; viz

$$1.006 \leq c_{p_d}(T) \leq 1011 \text{ kJ/kg } {}^oK$$

in the temperature range $0\ {}^oC \leq T \leq 80\ {}^oC$,

$$1.860 \leq c_{p_m}(T) \leq 1.884 \text{ kJ/kg } {}^oK$$

in the temperature range $7\ {}^oC \leq T \leq 87\ {}^oC$,

we have used for the specific heat calculations, the average values

$$\bar{c}_{p_d} = 1.008 \text{ kJ/kg } {}^oK$$

$$\bar{c}_{p_m} = 1.871 \text{ kJ/kg } {}^oK$$

In a small temperature range, $P_s(T)$ can be expressed by the following linear relationship:

$$p_s(T) = R_1 + R_2T \tag{33}$$

Consequently the humidity ratio defined by equ. (10) can be written as

$$W = 0.622\, r\, \frac{R_1 + R_2\, T}{p_1 - (R_1+R_2T)} \tag{34}$$

In the temperature range 10 ^oC to 70 ^oC, the values of R_1 and R_2, obtained through a least square fit, are given in table 7 along with the correlation with the exact values. It is obvious that the maximum change in the values of c_p in the temperature and relative humidity range of interest could be about seven percent maximum. The corresponding change in the thermal efficiency is also then about the same, i.e. a maximum of seven percent. It is also to be noted that these changes are the maximum possible one. Actual changes in the efficiency values are still of smaller magnitude. It is therefore not essential to incorporate the change of c_p with relative humidity for evaluating the efficiency of the collector, in particular when the aim is only to compare the performance of one collector from that of the other.

Table 7: Constants R_1 and R_2 obtained through a linear least square fit of the saturated pressure of water in a certain temperature range

T ^oC	R_1 atm	R_2 atm/deg	Correlation
10^o–30^o	$-4.788 \cdot 10^{-3}$	$1.487 \cdot 10^{-3}$	0.9888
30^o–50^o	$-8.316 \cdot 10^{-2}$	$4.014 \cdot 10^{-3}$	0.9920
50^o–70^o	$-3.616 \cdot 10^{-1}$	$9.484 \cdot 10^{-3}$	0.9930

6.8 Validity of Hottel-Bliss Equation

Equs. (17) and (19) are usually employed for characterising the performance of solar water /35, 44/ and solar air heating collectors /3,6,8,9/. For flat plate solar water heaters and for nonporous absorber type of air heaters, the factor F', F_R and heat loss coefficient U_L are nearly constant and a linear representationof

$$\eta \text{ vs} \left[T_f \; (= \frac{T_o + T_i}{2}) - T_a\right] I^{-1}$$

and vs $(T_i - T_a)$ plots provide a very useful method for specifying collector parameters like heat loss coefficient, effective absorptance-transmittance product, heat flow factor etc. For matrix air heaters also various authors /6,9/ have assumed the validity of eqs. (17) and (19) for characterizing their collectors.

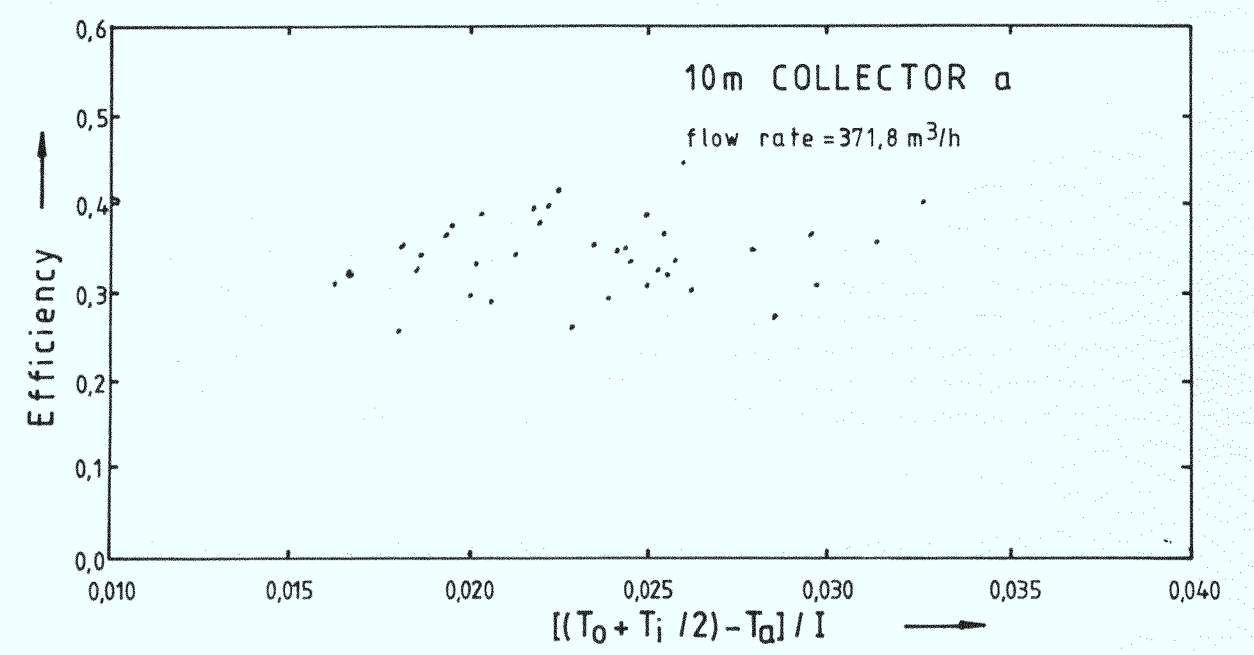

Fig.25: Variation of efficiency with $(T_f - T_a)/I$ for 10 m collector a.

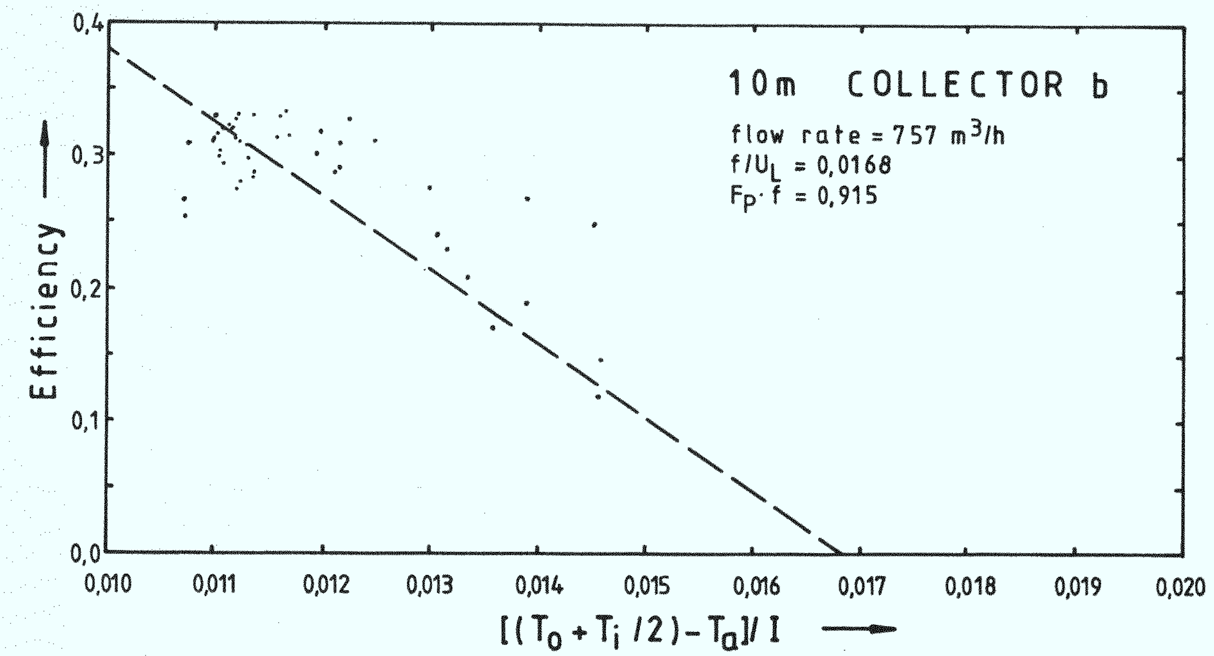

Fig.26: Variation of efficiency with $(T_f-T_a)/I$ for 10 m collector b

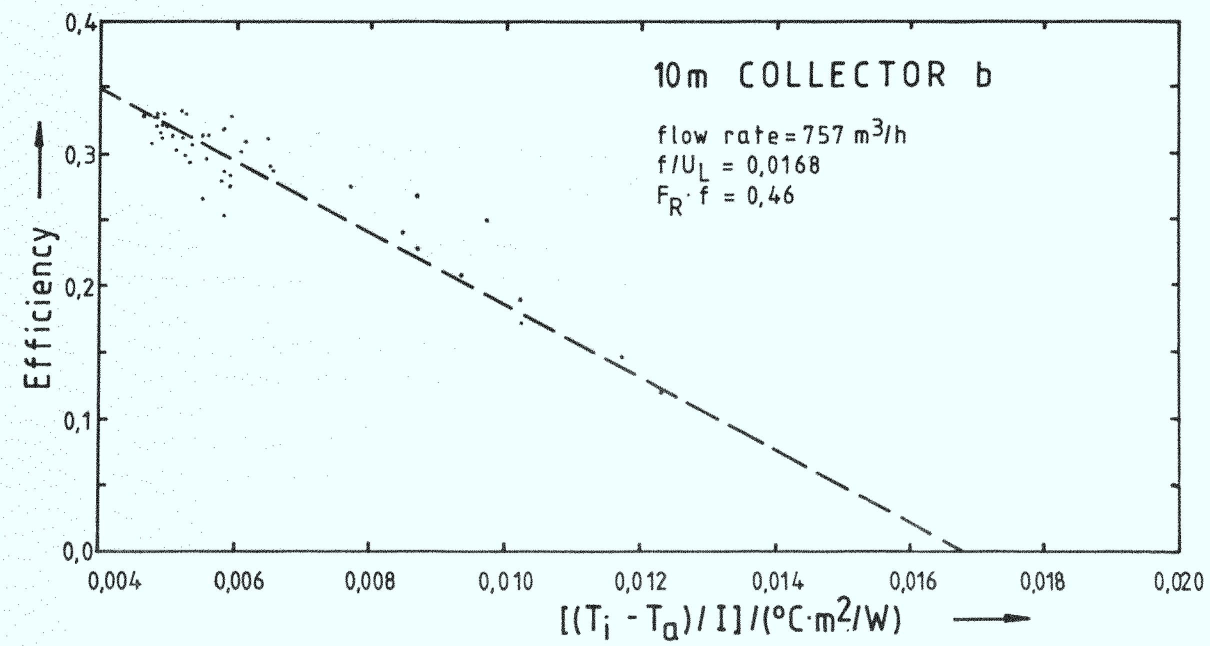

Fig. 27: Variation of efficiency with $(T_i-T_a)/I$ for 10 m collector b

We, however, observe that for 10 m collector a,

η vs $\frac{1}{I}\left[\left(\frac{T_o+T_i}{2} - T_a\right)\right]$ and η vs $\frac{1}{I}\left[(T_i - T_a)\right]$ plots cannot be approximated by a straight line. For illustration purposes we give a typical plot in Fig. 25 for an air flow rate of 371.8 m^3/h through the collector. For higher flow rates of air also, similar scattering of points is obtained. The reason for this wide scatter of points is the complicated nature of volumetric heat transfer in the matrix air heaters and the dependence of F' and F_R on the extinction coefficient of matrix, its thickness, conductivity of the absorber material etc. The mean fluid temperature also cannot be taken to be simply equal to

$$\frac{T_o + T_i}{2} .$$

Even for nonporous absorbers, if they are long solar collectors, the approximation T_f

$$T_f = \frac{T_o + T_i}{2}$$

is not strictly valid. The modified form of F', F_R and T_f for porous and nonporous solar air heaters shall be described elsewhere.

Figs. 26 and 27 show η vs

$\frac{1}{I}\left[\left(\frac{T_o + T_i}{2} - T_a\right)\right]$ and η vs $\frac{1}{I}\cdot\left[(T_i-T_a)\right]$ plots respectively

for 10 m collector b. It is interesting to see that for this collector the plots follow nearly a straight line thereby confirming our earlier results that the textile absorber of 10 m collector b essentially behaves as a nonporous type absorber.

7. CONCLUSIONS

Flexible mattress type of plastic solar air heater having a black porous polyester textile yield high thermal efficiency with reasonable high temperature increase. The important thing for such air heaters is an optimum pore density allowing a good flow of air and a good absorptivity of the solar radiation. The collector should be well insulated at the back.

Since the efficiency as high as about seventy percent is obtained, collecting nearly .65 kW/m^2 for a solar radiation of 900 W/m^2, with a temperature rise of nearly 20 ^oC, the collector can be put to a variety of applications. Apart from crop drying which is a natural application of any solar air heater, this collector can be used for domestic hot water heating, space heating and air conditioning. For the later applications it is desirable to have a closed loop cycle for the flowing air.

Acknowledgements

Authors are thankful to Dr. M. Meliß for his deep interest in this work and for providing necessary facilities to carry out the project. Stimulating discussions with him and with other colleagues, especially Dr. M. Kleeman, Dr. M. Grüter and Dr. Bundschuh at various stages of this work are gratefully acknowledged. The authors also like to thank the assistance of Mr. Schulz, Miss Schulze, Mr. Repschläger in carrying out this work. One of the authors (NKB) acknowledges the financial help of Alexander von Humboldt foundation during his stay in F.R.G.

REFERENCES

1 *M. Kudret Selcuk, Solar Air Heaters and their Applications, in Solar Energy Engineering, ed. by A.A.M. Sayigh, p. 155-182, Academic Press, N.Y. (1977)*

2 *G.O.G. Löf, Solar Air Systems in Solar Energy Conversion, ed. A.E. Dixon and J.D. Leslie, Pergamon Press, N.Y. (1979)*

3 *A.F. Whillier, Performance of black painted solar air heaters of conventional design, Solar Energy, 9 (1), 31-37 (1964)*

4 *D.J. Close, Solar air heaters for low and moderate temperature applications, Solar Energy, 7 (3), 117-124 (1963)*

5 *M.L. Khanna and N.M. Singh, Industrial solar drying, Solar Energy 11 (2), 1967*

6 *C.L. Gupta and H.P. Garg, Performance Studies on Solar Air Heaters, 11 (1), 25 (1966)*

7 *P.K. Bansal and S.C. Kaushik, Analysis of single and double exposure solar air heaters, Energy Research, 4(1), 69 (1980)*

8 *B.F. Parker, Solar collector design and performance. Paper No. 80-4035, Summer meeting of American Society of Agricultural Engineers, St. Joseph, Michiga 49085*

9 *B.F. Parker, Derivation of efficiency and loss factors for solar air heaters, Solar Energy, 26, 27-32 (1981)*

10 *J.P. Chiou at al., A Slit and Expanded Aluminium Foil Matrix Solar Collector, Solar Energy, 9(2), 83-80 (1965)*

11 *W.A. Beckmann, Raidation and Convection Heat Transfer in Porous Bed, J. Eng. Power, January, 51-54, ASME (1968)*

12 *Y.H. Hamit and W.A. Beckmann, Transpiration Cooling and Radiatively Heated Porous Bed, ASME Paper No. 69-WA/Sol 6.*

13 *M.K. Selcuk, Solar Air Preheater and Fruit Drier, Comples Bull, No. 10, 79-82 (1966)*

14 *M.K. Selcuk, Final Report of the Solar Fruit Drier, Comples Bull, No. 12, 91-101 (1967)*

15 *M. Akyrt, A Solar Dehydrator for Orchards, Comples Conf. Istanbul, Turkey, September (1972)*

16 *F.L. Lansing and V. Clarke, A high performance porous flat plate solar collector, Energy, 4, 685-694 (1979)*

17 *D. Singh, S.S. Bharadwaj and N.K. Bansal, Thermal Performance of Matrix Air Heater, Energy Conversion and Management, 21, 253 - 256 (1981)*

18 *M.S. Sodha, N.K. Bansal, D. Singh and S.S. Bharadwaj, Thermal Analysis of a Matrix Air Heater. International Journal of Energy (in press)*

19 *A. Blaga, Use of Plastics in Solar Energy Applications, Solar ENergy 21, 331-338 (1978)*

20 *A.F. Boeckmann, Collectors, Pipes and Heat Accumulators made of Plastic, 2nd Meeting on Fundamentals of Solar Engineering, 1. Fellbach, FRG, 22nd Oct. (1976). J.W. Andrews and W.G. Wilhelm, Thin film flat plate solar collectors for low cost manufacture and installation, BNL-51124, Brookhaven National Laboratory, Upton, N.Y. (1980)*

21 *W.G. Wilhelm, Low Cost Solar Collectors Using Thin Film Plastics, Absorbers and Glazings. F.L. Weichman and D.G. Hughes, 3rd Conference of the Solar Energy Society of Canada, Edmonton,Alberta, Canada, 22nd Aug., 1977 (1977)*

22 *F.L. Weichmann and D.G. Hughes, Direct absorption solar collector, 3rd conference of the Solar Energy Society of Canada, Edmonton, Alberta, p.15, paper No. 40 (1977)*

23 *R.G. Sarazin and L.D. Olson, U.S. Patent 4,023,556, to Universal Oil Products Co., p. 4. 17th May 1977 Filed date 27th May 1975.*

24 *J.P. Chiou, Polyolefin Plastic Solar Collector and Its Applications in Cold Climates, Solar Energy in Cold Climates, Detroit, Michigan (USA), p. 172-182 (1976)*

25 R.A. Erb, Unitary Solar Collector - a New Approach to Low-cost Flat-plate Systems, International Solar Energy Society Meeting. Atlanta, GA, USA, SUNII ed. by K.W. Boer and B.H. Glenn, 338-341, Pergamon Press Inc., N.Y. (1979)

26 E.J. Hojnowski, Solar Heat Collector Panel, US Patent 3 995,615 (1976)

27 T. Kay, Solar Collector Panel and Refrigeration System Operated thereby, US Patent 4,126,014, p. 6, 21st Nov. 1978

28 A. Boettcher and E. Delyannis, Development of a solar air collector, Statusbericht Sonnenenergie Vol. I, 95-101, Verein Deutscher Ingenieure (1980)

29 H. Schulz, Überprüfung von Einfach-Luftkollektoren (Luftkollektor Test), Statusbericht Sonnenenergie Vol. I, 171-181, Verein Deutscher Ingenieure (1980)

30 P.J. Lunde, Solar thermal engineering, John Wiley and Sons, N.Y. (1980)

31 Meßstrecken und Fassungsringe, DIN 19205, Beuth Verlag GmbH, Berlin (FRG) (1975)

32 Elektrische Thermometer, DIN 43760, Oktober 1980, Deutsches Institut für Normung, Berlin

33 J.W. Grüter, SOLARNET Ein Datenerfassungs- und Kommunikationssystem für Experimente der Solarenergieanwendung bei der KFA, KFA Interner Bericht, KFA-IKP-STE IB 6-81 (1981)

34 Möller, F., Einführung in die Meteorologie, p. 127-133, Bi Hochschultaschenbücher Bd. 276, Mannheim 1973

35 BSE Working Group. "Usability of Solar Collectors", Part A: Solar Collector Efficiency Test, p. 37-39, May 1978, 43 Essen 1, Kruppstr. 5, Fed. Rep. of Germany

36 Firma Thies, Klein-Windmesser, 34 Göttingen, Fed. Rep. of Germany

37 Repschläger, H., "Die Windgeschwindigkeitsmessung bei der Standortbestimmung für Windenergieanlagen", Interner Bericht, KFA-STE-IB-3/81 KFA, 517 Jülich, Fed. Rep. of Germany

38 J.W. Grüter, H. Ringel, MADAS, Ein Datenerfassungssystem auf Mikroprocessorbasis, Int.Ber., KFA, 517 Jülich, Fed. Rep. of Germany

39 H.C. Hottel and A. Whillier, Transactions of the Conference on the Use of Solar Energy, Vol. 2, Part I, p. 74, University of Arizona Press (1958)

40 R.W. Bliss, "The Derivation of Several Plate Efficiency Factors, Useful in the Design of Flat Plate Solar Heat Collectors, Solar Energy 3 (4), 55 (1959)

41 *A.J. Duffie and W.A. Beckmann, Solar Energy Thermal Processes, p. 164-165, John Wiley and Sons, N.Y. (1976)*

42 *K. Hammecke, G. Pietralla and K.H. Presser, Thermodynamische Stoffwerte von Luft, Kohlendioxid und Stickstoff bei hohen Temperaturen und Drücken, Jül-303-RB, Kernforschungsanlage Jülich, Jülich, FRG (1966)*

43 *Tables of thermodynamic and transport properties of air, argon, carbonmonoxide, hydrogen, nitrogen, oxygen and steam. Pergamon Press, N.Y. (1960)*

44 *J.E. Hill and T. Kusuda, Method of testing for rating solar collectors based on thermal performance, NBSIR 74-635, National Science Foundation, Washington, USA (1974)*

45 *E. Sprenger, Taschenbuch für Heizung und Klimatechnik, R. Oldenbourg München Wien (1979)*

NOMENCLATURE

Symbol	Physical Quantity	Units
A	Collector area	m^2
A_d $(= \frac{\pi d^2}{4})$	Area of the aperture opening	m^2
A_o	Numerical constant	dimensionless
B	Numerical constant	dimensionless
C	Numerical constant	dimensionless
C_p	specific heat of atmospheric air	J/kg K
C_{p_d}	specific heat of dry air	J/kg K
C_{p_m}	specific heat of water vapour	J/kg K
D	Numerical constant	dimensionless
d	Diameter of the aperture opening	m
h	Pressure drop across the aperture	mm of water
I	Solar intensity	W/m^2
L_V	Latent heat of vapourisation	cal/g
$\dot{m}$	Volume of air flow per unit time	m^3/h
$\dot{m}_w$	Mass of air flow per unit time	kg/s
n	Number of mols	dimensionless
p	Static pressure of the air	atm
p_o	Static pressure of air at 273 ^oK	atm
P_A	Atmospheric pressure	Torr
P_{el}	Electrical power consumed by fan	W
P_S	Saturated vapour pressure	Torr
P_V	Real vapour pressure	Torr
q_u	useful thermal power	W
Q_u	Net useful power	W
r	Relative humidity	dimensionless
R	Gas constant	J/mol K
R_t	Resistance of platinum temperature feeler at θ ^oC	Ω

R_o	Resistance of platinum temperature feeler at 0 ^oC	Ω
T_a	Atmospheric temperature	^oC
T_d	Dry bulb temperature	^oC
T_f	Mean fluid temperature	^oC
T_i	Inlet air temperature	^oC
T_o	Outlet air temperature	^oC
T_w	Wet bulb temperature	^oC
U_L	Heat loss coefficient	$W/m^2\ ^oC$
v	Wind speed	m/s
V	Volume of the air	m^3
W	Humidity ratio	dimensionless
Z	Compressibility of air	dimensionless
$(\tau\alpha_a)_e$	Effective transmittivity absorptivity product	dimensionless
η	Thermal efficiency	dimensionless
ΔP	Pressure drop across the aperture	mm of H_2O
ρ	Density of air	kg/m^3
$\tau_2 - \tau_1$	Time interval	sec